Nuclear Myosin 1 regulates platelet activation and immune response: A novel therapeutic target for hematologic disorders

[1,2]Tomas Venit, [3]Samira Khalaji, [1,4]Valentina Fambri, [1,5]Wael Abdrobou, [6]Mei El Gindi, [1]Rahul Shrestha, [2]Pavel Hozak, [1,3]Youssef Idaghdour, [6]Jeremy CM Teo and [1,3,7]Piergiorgio Percipalle

[1]Program in Biology, Division of Science and Mathematics, New York University Abu Dhabi (NYUAD), P.O. Box 129188, Abu Dhabi, United Arab Emirates; [2]Laboratory of Biology of the Cell Nucleus, Institute of Molecular Genetics, Czech Academy of Sciences, Prague, Czech Republic; [3]Center for Genomics and Systems Biology, New York University Abu Dhabi (NYUAD), P.O. Box 129188, Abu Dhabi, United Arab Emirates; Abu Dhabi University, College of Health Sciences, Abu Dhabi, United Arab Emirates; [4]Department of Biology, New York University, NY, USA; [5]College of Health Sciences, Abu Dhabi University, Abu Dhabi, United Arab Emirates; [6]Laboratory for Immuno Bioengineering Research and Applications Division of Engineering, New York University Abu Dhabi, Saadiyat Campus, P.O. Box 127788, Abu Dhabi, United Arab Emirates

[7]Correspondence: Piergiorgio Percipalle, address as above

Tel.: +97126284389

Email: pp69@nyu.edu

Keywords: platelet activation, blood coagulation, immune response, transcriptional regulation, metabolic reprograming, mitochondria, stem cells, Nuclear Myosin 1

Abstract

Cellular differentiation involves complex events associated with changes in cellular shape, function and proliferative capacity. This process is regulated by specific expression of multiple genes, which guide the cell through differentiation but also ensure proper function of terminal cell types. Over the last decade, the role of cellular metabolism in maintaining stem cells pluripotency and differentiation has been getting more attention due to a direct link between metabolic state and differentiation potential of cells. Since Nuclear Myosin 1 (NM1) deletion leads to a switch from oxidative phosphorylation to aerobic glycolysis and tumorigenesis in mice, here we asked if NM1 also contributes to cell differentiation. Indeed, analysis of metabolomic profiles and cytokine and chemokine levels upon NM1 depletion support a role in hematopoiesis. In an NM1 KO mouse model results from total blood cell count and bleeding assay show decreased erythropoiesis and thrombopoiesis as well as failure in hemostasis. Next, we explored the role of NM1 during the differentiation of hematopoietic progenitor stem cells to terminal blood cells by transcriptionally profiling bone marrow, spleen and peripheral blood from NM1 KO mice. We found that in bone marrow, NM1 deletion leads to overexpression of genes associated with glycolysis-dependent platelet activation and suppression of the innate immune system. These expression patterns are preserved and become more complex in spleen and peripheral blood. The study, therefore, provides insights into the underlying mechanisms of hematopoietic differentiation and activation of specific blood cell types and suggests NM1 as a potential therapeutic target for blood-related disorders.

45 **Introduction**

46 Nuclear Myosin 1 (NM1) belongs to the family of unconventional single-headed myosins present
47 in the cytoplasm and the cell nucleus. Myosins are involved in various processes such as regulation of the
48 plasma membrane and actin cytoskeleton, exocytosis of vesicles, cell movement, repair of DNA damage
49 foci, movement of the chromatin, and transcription regulation. NM1 was the first myosin discovered in
50 the cell nucleus, and over the years, several studies described its general roles and mechanism of function
51 in Polymerase I, II, and III transcription (1, 2). NM1 is one of three alternatively spliced isoforms of the
52 Myo1C gene exhibiting an extra 16 amino-acid stretch on its N-terminus. All Myo1C isoforms share the
53 same nuclear localization signal and partially overlap in function (3, 4). In the cell nucleus, NM1 has been
54 shown to directly bind to the chromatin at the transcription start site, forming a complex with actin and
55 the polymerase machinery, which is later on released and replaced by NM1 binding to the chromatin
56 remodeling complex B-WHICH via direct interaction with the ATPase subunit SNF2H (5, 6). This leads to
57 chromatin remodeling around the transcription start site but also to NM1 association with the histone-
58 acetyl- and histone-methyl-transferases PCAF and Set1, respectively. They acetylate and methylate
59 surrounding histones as a mark for active transcription and allow polymerase-mediated transcription.
60 Recently, we reported that these mechanisms are important for numerous cellular functions, including
61 the transcriptional response to DNA damage (7). Mechanistically, we discovered that NM1 is part of the
62 DNA damage signaling cascade as it interacts with p53 to activate transcription of the cell cycle regulator
63 p21 (Cdkn1A). Upon DNA damage, p53 binds to its responsive promoter upstream of the Cdkn1A gene
64 followed by NM1-dependent acetylation and methylation of surrounding H3 histones. This allows for
65 rapid p21 protein accumulation and cell cycle arrest until DNA damage is repaired, while cells missing
66 Nuclear myosin 1 accumulate DNA damage and are prone to apoptosis (2, 7).

67 In a more recent study, we reported a novel role for NM1 as a tumour suppressor and regulator
68 of cellular metabolism. The conventional view of somatic cells using only oxidative phosphorylation and

69 cancer cells using only aerobic glycolysis as a primary type of metabolism was widely disproved over time.
70 In many cases, both types of metabolism coexist in cells, with their ratio adjusting based on the acute
71 needs. For example, pluripotent stem cells, in many ways resembling cancer cells, use aerobic glycolysis
72 as the primary energy source, but upon differentiation, they gradually move towards oxidative
73 phosphorylation, which becomes a dominant metabolic pathway. However, some fully differentiated
74 somatic cells can still rely on aerobic glycolysis as their primary energy source or switch between the two
75 metabolic pathways depending on the surrounding environment. We showed that NM1 is part of the
76 nutrient-sensing PI3K/Akt/mTOR pathway, forming a positive feedback loop with mTOR. NM1 deletion
77 leads to a suppression of mitochondrial transcription factors TFAM and PGC1α, negatively regulating
78 mitochondrial oxidative phosphorylation and leading to metabolic reprogramming towards aerobic
79 glycolysis associated with cancer cells. Indeed, NM1 knockout (KO) cells can form solid tumours in a nude
80 mouse model even though they have suppressed the PI3K/Akt/mTOR signalling pathway, suggesting that
81 the metabolic switch towards aerobic glycolysis provides a sufficient signal for carcinogenesis (8).
82 Seeing that NM1 regulates cellular metabolism by influencing the transcription of mitochondrial
83 transcription factors, in this study, we investigated whether NM1 deletion affects the ability of pluripotent
84 stem cells to differentiate into terminal somatic cells. Additionally, we examined whether NM1 impacts
85 the functionality of specific cell types that rely on active switching between two metabolic pathways. To
86 address this, we used hematopoiesis as a model system since hematopoietic stem cells (HSCs) give rise to
87 a wide variety of highly specialized blood cells with specific energetic needs. In general, these cells are
88 present in the bone marrow, and they are generated from hematopoietic lineages with progenitor
89 hematopoietic stem cells (HSCs) giving rise to red blood cells, white blood cells, and platelets. All other
90 cell types are components of the bone marrow stroma and are involved in the formation of specific
91 microenvironments regulating HSCs. The cell types present in bone marrow stroma include mesenchymal
92 stem cells, fibroblasts, adipocytes, osteoblasts, osteoclasts, and endothelial cells (9). From the metabolic

93 perspective, hematopoietic stem cells use anaerobic glycolysis as the only energy source and switch to
94 oxidative phosphorylation only during differentiation (10). The energy metabolism of fully differentiated
95 hematopoietic cells depends on their function. Erythrocytes lose their nucleus and mitochondria during
96 differentiation, making them entirely reliant on glycolysis for energy production (11). Monocytes use
97 oxidative phosphorylation as the primary energy source. However, they switch to glycolysis upon
98 activation to pro-inflammatory M1 macrophages and back to oxidative phosphorylation upon switching
99 to anti-inflammatory M2 macrophages (12, 13). Like monocytes, lymphocytes use oxidative
100 phosphorylation in their quiescent state and switch to glycolytic metabolism only upon activation (14). In
101 contrast, neutrophils use glycolysis, and their limited mitochondria serve only for apoptotic signaling (15).
102 Finally, platelets (thrombocytes), derived from the cytoplasmic fragmentation of megakaryocytes and
103 essential for blood coagulation at injury sites, utilize both oxidative phosphorylation and glycolysis for
104 energy production. However, their activation depends on aerobic glycolysis (16, 17). The bone marrow
105 stromal cells follow similar metabolic patterns as hematopoietic lineages, and mesenchymal stem cells
106 use glycolysis as a primary source of metabolism (18). Differentiation of these cells to osteoblasts,
107 however, is not associated with metabolic switch to oxidative phosphorylation, and osteoblasts use
108 glycolysis to produce ATP (19). In contrast, osteoclasts, which originate from hematopoietic monocytes,
109 rely on oxidative phosphorylation during differentiation and maturation but switch to glycolytic
110 metabolism only upon activation (20, 21).

111 By using NM1 wild type (WT), knock-out (KO) and NM1-rescued (KO+NM1) mouse embryonic
112 fibroblasts (MEFs), as well as NM1 WT and KO mice, here we show evidence that NM1 deletion leads to
113 alterations in signature metabolites implicated in hematopoiesis and differential gene expression of genes
114 involved in platelet activation and immune system response. In an NM1 KO mouse we show decreased
115 erythropoiesis and thrombopoiesis associated with failure in hemostasis. Consistent with our previous
116 results, showing the shift towards glycolysis in NM1 KO cells, we show that glycolysis-dependent platelet

117 activation is upregulated upon NM1 deletion in bone marrow and peripheral blood. In contrast, the innate
118 immune system response is suppressed in NM1 KO mice, which can be associated with the need for
119 oxidative phosphorylation during differentiation of several innate immune cells, like monocytes, dendritic
120 cells, or mast cells. In agreement with it, bead-based immunoassays show that the excretion of several
121 cytokines and pro-inflammatory chemokines is abolished in NM1 KO cells. In the spleen, innate immune
122 system genes are suppressed as well, while adaptive immune system genes, mostly associated with T-cell
123 activation and T-regulatory cell (Treg) differentiation, are upregulated, which is consistent with the
124 metabolic need for aerobic glycolysis in these cells.
125

126 **Material and Methods**

127 **Cell lines**.

128 Nuclear Myosin 1 Knock-Out (NM1 KO) cell lines were derived from wild-type mouse embryonic
129 fibroblasts (MEFs) (ATCC® CRL-2752) (NM1 WT) using the CRISPR/Cas9 system (7). The rescue cell line
130 expressing exogenous NM1 in NM1 KO MEFs (NM1 KO+NM1) was prepared previously by lentiviral
131 transduction of vector carrying coding sequence for NM1 fused with HA and V5 tag (VectorBuilder) (8).
132 Actin WT and KO cells were described previously (22, 23). Cells were grown in a DMEM medium containing
133 10% fetal bovine serum, 100 U/ml penicillin, and 100 mg/ml streptomycin (Millipore-Sigma) in a
134 humidified incubator with 5% CO_2 at 37 °C.

135 **Large-scale Ultra-Performance Liquid Chromatography High-Resolution Mass Spectrometry**.

136 5 replicates of $3x10^5$ overnight grown NM1 WT and KO cells were used for metabolomic profiling. Cells
137 were washed twice with ice-cold 0.9% NaCl solution and then incubated on ice for 3 minutes in 300µl of
138 100% Methanol. Subsequently, cells were scraped using a precooled cell scraper, moved to a cold
139 Eppendorf tube, and spun down at 15000rpm for 15 min at 4°C. 200µl of each supernatant was used for
140 further processing. Samples were vacuum dried and reconstituted in 200µl of cyclohexane/water (1:1)
141 solution for subsequent analysis by Ultra Performance Liquid Chromatography High-Resolution Mass
142 Spectrometry (UPLC-HRMS) performed at the VIB Metabolomics core facility (Belgium). 10 ul of each
143 sample were injected on a Waters Acquity UHPLC device connected to a Vion HDMS Q-TOF mass
144 spectrometer. Chromatographic separation was carried out on an ACQUITY UPLC BEH C18 (50 × 2.1 mm,
145 1.7 µm) column from Watersunder under the constant temperature of 40°C. A two-buffer gradient was
146 used for separation: buffer A (99:1:0.1 water:acetonitrile:formic acid, pH 3) and buffer B (99:1:0.1
147 acetonitrile:water: formic acid, pH 3), as follows: 99% A for 0.1 min decreased to 50% A in 5 min, decreased
148 to 30% from 5 to 7 minutes, and decreased to 0% from 7 to 10 minutes. The flow rate was set to 0. 5 mL

149 min−1. Both positive and negative Electrospray Ionization (ESI) were applied to screen for a broad array
150 of chemical classes of metabolites present in the samples. The LockSpray ion source was operated in
151 positive/negative electrospray ionization mode under the following specific conditions: capillary voltage,
152 2.5 kV; reference capillary voltage, 2.5 kV; source temperature, 120°C; desolvation gas temperature,
153 600°C; desolvation gas flow, 1000 L h−1; and cone gas flow, 50 L h−1. The collision energy for the full MS
154 scan was set at 6 eV for low energy settings, for high energy settings (HDMSe) it was ramped from 28 to
155 70 eV. The mass range was set from 50 to 1000Da, scan time was set at 0.1s. Nitrogen (greater than 99.5%)
156 was employed as desolvation and cone gas. Leucine-enkephalin (250 pg/µL solubilized in water:
157 acetonitrile 1:1 [v/v], with 0.1% formic acid) was used for the lock mass calibration, with scanning every 1
158 min at a scan time of 0.1 s. Profile data was recorded through Unifi Workstation v2.0 (Waters).

159 **Unsupervised Metabolomics Data Analysis**.

160 Raw MS peak intensity data representing the abundance of detected metabolic features were subject to
161 data integrity check. Metabolic features with a constant or single value across all samples were removed.
162 Missing values, if detected, were replaced by 1/5 of the minimum positive values of their corresponding
163 variables. Data filtering was performed to remove non-informative features that are considered baseline
164 noise. Features that are near-constant throughout experimental conditions were detected using standard
165 deviation (SD) and removed from downstream analysis (24). Filtered data were subject to sample median
166 normalization to adjust for systematic differences among samples. Data were then log-transformed (base
167 10) to deal with negative values after the normalization. Pareto scaling was used to adjust each metabolic
168 feature by a scaling factor computed based on the dispersion of the variable (mean-centered and divided
169 by the range of each variable). PCA and hierarchical clustering were done to explore the correlation
170 structure in the data across the two experimental conditions (WT and KO). Data QC, filtering, and
171 unsupervised statistical analysis were performed using MetaboAnalyst v6.0 (25). An unpaired t-test was
172 used to detect differential abundant metabolic features between the experimental conditions.

173 **Functional and metabolic pathway enrichment analysis**.

174 Functional analysis of curated normalized peak intensity data was performed using MetaboAnalyst v6.0
175 using an existing protocol (25). Implemented Gene Set Enrichment Analysis (GSEA) method in the
176 Functional Analysis module of MetaboAnalyst v6.0 (Accessed in 2024 from
177 http://www.metaboanalyst.ca/) was used to identify sets of functionally related compounds and evaluate
178 their enrichment of potential functions defined by metabolic pathways. GSEA analysis of compounds
179 identified using positive and negative ionization was performed separately. Putative annotation of MS
180 peaks data considering different adducts and ion modes was performed. *m/z* values and retention time
181 dimensions were used to increase confidence in identifying compounds and improve the accuracy of
182 functional interpretations. Annotated compounds were then mapped onto Mus musculus (mouse)
183 [BioCyc] (26-28) for pathway activity prediction (Supplementary Table 1 and 2). GSEA calculates the
184 Enrichment score (ES) by walking down a ranked list of metabolites, increasing a running-sum statistic
185 when a metabolite is in the metabolite set and decreasing it when it is not. A metabolite set is defined in
186 this context as a group of metabolites with collective biological functions or common behaviors,
187 regulations, or structures. In this method, the ES of each enriched pathway is calculated to reflect the
188 degree to which a metabolite set is overrepresented at the top or bottom of a ranked list of metabolites.
189 Each ES is then normalized by the average of all ES scores against all permutations of the expression
190 dataset to generate normalized enrichment scores (NES) that are used to compare analysis results across
191 metabolite sets. By normalizing the enrichment score, GSEA accounts for differences in metabolite set
192 size and correlations between metabolite sets and the expression dataset. A positive NES indicates that
193 the enriched metabolite set is at the top of the ranked list; a negative NES indicates that the enriched
194 metabolite set is at the bottom of the ranked list (28). Finally, compound hits were identified for each
195 enriched pathway. Raw metabolomic data are publicly available in the Mendeley database
196 (https://data.mendeley.com/preview/nxzs4dtztg?a=aecce665-2b58-4a98-8328-b70d689c249a).

197 **Chemokine and cytokine measurement**.

198 NM1 WT, NM1 KO, and NM1 KO+NM1 were used for the analysis. 5x 10^5 cells per well were seeded in 24
199 well plates and left to grow for 48 hours under standard conditions. Next, cells were spun down on plates
200 to remove debris and media used for subsequent analysis of chemokine and cytokine content by the bead-
201 based immunoassays LEGENDplexTM Mouse Cytokine Panel 2 (740134) and LEGENDplexMU
202 Proinflammatory Chemokine Panel (both BioLegend) according to manufacturer's protocol. In short, 25µl
203 of media from each cell type was incubated for 2 hours with a combination of different capture beads
204 bound to specific antibodies detecting given chemokine/cytokine. After a series of washes, biotinylated
205 detection antibodies were added to each sample plate to form capture bead-analyte-detection antibody
206 sandwiches. Next, streptavidin-phycoerythrin (SA-PE) was added to the mixture to be bound to the
207 biotinylated detection antibodies, providing fluorescent signal intensities in proportion to the number of
208 bound analytes. Samples were then analyzed by flow cytometer, where specific beads were differentiated
209 by size and internal fluorescence intensity, and analyte-specific populations were segregated and
210 quantified by the PE fluorescent signal. The concentration of a particular analyte was determined by a
211 standard curve generated in the same assay. For each cell type, 6 biological replicates were used for the
212 measurement and each measurement was performed in 2 technical replicates. The final concentration of
213 the given analyte in each biological replicate is calculated as a mean value between 2 technical replicates.

214 **Isolation of tissues from mice and isolation of RNA**.

215 Wild type (WT) and NM1 KO C57/Bl6 mice (8 months old; 25-35 g in weight) were used for the analysis
216 (29). The mice were housed in a pathogen-free sterile ventilation system supplied with sterile woodchip
217 and *ad libitum* feed and water supply. Mice were kept in a room maintained at a temperature of 21-24 °C
218 on a schedule of 12 h light/dark cycle. All animal experiments were performed after approval by the
219 NYUAD-IACUC (Protocol 20-0004, 23-0009).

220 For the transcriptomic analysis we used bone marrow tissue as an example of the primary lymphoid organ
221 where hematopoietic differentiation happens, the spleen as an example of a secondary lymphoid organ
222 where specific mature cell types reside, and are activated upon stimulus, and peripheral blood as the site
223 of action for circulating blood cells. Bone marrow was isolated according to the previously published
224 protocol (30). In short, femurs and tibiae were taken from euthanized mice and cleaned from surrounding
225 muscles, connective tissues, and epiphysis parts of each long bone. All bones from single mice were placed
226 in the 0.5ml tube with the hole on the bottom nested in the 1.5ml collection tube. Bones were spun down
227 at 14000 x g in a microcentrifuge for 15 seconds to pellet the bone marrow at the bottom of the bigger
228 tube. For each bone marrow sample, femurs and tibiae from single NM1 WT or KO mice were used. RNA
229 was isolated by RNAzol according to the manufacturer's protocol. Spleen was isolated from euthanized
230 mice and cleaned from surrounding fat and connective tissue. Approximately 5mm^3 of tissue from the tip
231 of the spleen was merged in RNAzol and homogenized in bead mill homogenizer followed by standard
232 RNA isolation protocol. Blood samples were collected by submandibular vein bleeding according to a
233 previously published protocol (31). Collected blood was immediately mixed with the double amount of
234 RNAzol and samples were thoroughly mixed and stored on dry ice before RNA isolation by standard
235 protocol. The final RNA concentration was measured by the Qubit RNA BR Assay Kit.

236 **RNA-Seq library preparation, sequencing, and analysis**.

237 Three replicates were prepared for each tissue and each genotype. 500ng of total RNA was used for RNA-
238 Seq library preparation with the NEBNext Ultra II RNA Library Prep Illumina Kit (NEB) and sequenced with
239 the NextSeq 500/550 sequencing platform (performed at the NYUAD Sequencing Center within the
240 NYUAD Core Technology Platform). Subsequent analysis, including quality trimming, was executed using
241 the BioSAILs workflow execution system. Trimmomatic (version 0.36) was used for quality trimming of the
242 raw reads to get rid of low-quality bases, systematic base-calling errors, and sequencing adapter
243 contamination(32). The quality of the sequenced reads pre/post quality trimming was assessed by FastQC

244 and only the reads that passed quality trimming in pairs were selected for downstream analysis
245 (https://www.bioinformatics.babraham.ac.uk/projects/fastqc/). The quality-trimmed RNA-Seq reads
246 were aligned to the Mus musculus GRCm38 (mm10) genome using HISAT2 (version 2.0.4)(33). The
247 conversion and sorting of SAM alignment files for each sequenced sample to BAM format were done by
248 using SAMtools (version 0.1.19)(34). The BAM alignment files were processed using HTseq-count, using
249 the reference annotation file to produce raw counts for each sample. The raw counts were analyzed using
250 the NASQAR online analysis tool (http://nasqar.abudhabi.nyu.edu/), to merge, normalize, and identify
251 differentially expressed genes (DEG) as well as for the production of PCA and MA plots. DEG with log2(FC)
252 ≥ 0.5 and adjusted p-value of <0.05 for upregulated genes, and log2(FC) ≤ −0.5 and adjusted p-value of
253 <0.05 for downregulated genes between the NM1 WT and KO samples for each tissue were used for the
254 gene ontology (GO) enrichment analysis using DAVID Bioinformatics (https://david.ncifcrf.gov/)(35). RNA-
255 Seq data were deposited in the Gene Expression Omnibus (GEO) repository under accession number
256 GSE293993. Gene ontology bar charts and gene expression heatmaps were produced in GraphPad Prism
257 8.3.0 software. The STRING database was used for the production of an interaction map based on text
258 mining, experimental data, co-expression, and database search (36).

259 **Bleeding Time (BT) Test**

260 To assess primary hemostasis and to investigate the effect of NM1 on platelet function, bleeding time was
261 measured following tail-tip transection. Briefly, 2 mm of the distal tail tip was amputated, and the bleeding
262 site was gently blotted every 15 seconds using the rough side of filter paper without applying pressure to
263 the wound. The procedure continued until no further blood appeared on the filter paper. Bleeding time
264 (in seconds) was calculated by multiplying the total number of blood spots by 15. The physiological
265 bleeding time range in mice typically falls between 2 to 7 minutes (37).

266 **Complete Blood Count (CBC)**

267 Whole blood was collected from 12-month-old mice via cardiac puncture into EDTA-coated tubes to
268 prevent coagulation. Haematological parameters were analysed using an automated BeckmanDxH 900
269 Haematology Analyzer according to the manufacturer's instructions. Platelet count (PTL), white blood cell
270 count (WBC), red blood cell count (RBC), and unclassified white blood cells (UWBC) were measured.
271 Differential WBC counts, including neutrophils, lymphocytes, monocytes, eosinophils, basophils, and
272 nucleated red blood cells (NRBC), were also recorded. Additional parameters, including hematocrit (HCT),
273 hemoglobin concentration (HGB), mean corpuscular volume (MCV), mean corpuscular hemoglobin
274 (MCH), mean corpuscular hemoglobin concentration (MCHC), red cell distribution width (RDW and RDW-
275 SD), and mean platelet volume (MPV), were evaluated to assess platelet numbers and overall
276 haematological profiles in both WT and KO mice.

277

278 **Results**

279 **Hematopoietic signature metabolites are dysregulated in NM1-depleted mouse embryonic fibroblasts.**

280

281 To study the impact of NM1 on metabolic processes, we performed Liquid Chromatography followed by
282 High-Resolution Mass Spectrometry of cellular extracts from WT and NM1 KO MEFs. A total of 15,423
283 features were detected, and the quality control of the peak intensity data resulted in the retention of
284 9,193 and 5,425 metabolic features detected using positive and negative ionization, respectively.
285 Principal-component analysis (PCA) of the normalized peak intensity data detected using positive
286 ionization revealed a strong correlation structure in the metabolomic data across both conditions with
287 the first two PCs explaining 66.0% of the variation in the dataset (Supplementary Figure 1A). Similarly,
288 PCA of normalized peak intensity data detected using negative ionization revealed a strong correlation
289 structure in the metabolomic data across both conditions with the first two PCs explaining 61.5% of the
290 variation in the negative ionization dataset (Supplementary Figure 1B), capturing the effect of loss of NM1
291 and showing clear segregation between replicates of the WT and KO. Next, we used an unpaired t-test to
292 investigate differentially abundant metabolic features between NM1 WT and KO cells. Clustering of the
293 top 50 significantly differentially abundant metabolic features between the two conditions clearly shows
294 that replicates of each condition cluster together and NM1 deletion leads to distinct metabolomic changes
295 in these cells in both datasets using the two ionization methods (Supplementary Figure 1C and 1D).
296 To identify perturbations in mouse-specific metabolic pathways or metabolite sets in association with the
297 loss of NM1, functional analysis using the Gene Set Enrichment Analysis (GSEA) approach was performed
298 for metabolic features detected using positive and negative ionization and mapped onto Mus musculus
299 (mouse) [BioCyc], separately. The analysis of the positive ionization dataset revealed the enrichment of
300 polyamine biosynthesis pathways (Spermine biosynthesis I and II, and Spermidine biosynthesis pathways,
301 NES score = 1.281, *p-value* = 0.04; Supplementary Table 3 and Figure 1A). Particularly, the analysis

302 revealed a significant increase in the abundance of 5-methylthioadenosine (MTA) in the NM1 KO Cells (*t*
303 = 6.55, *p* value = 0.0002; Supplementary Table 1 and 3, and Figure 1C). The significant increase in the
304 levels of MTA, the S-methyl derivative of adenosine, in the NM1-KO cells reveals significant perturbations
305 in the methionine salvage pathway, which is universal to aerobic life (38, 39). Importantly, MTA, a
306 naturally occurring nucleoside, plays a significant role in modulating platelet aggregation. It has been
307 shown that MTA and its analogs regulate platelet aggregation through its influence on adenosine signaling
308 pathways. MTA has been shown to elevate intracellular cAMP levels, which subsequently inhibits platelet
309 aggregation. This mechanism operates independently of the P2Y12 receptor, a key player in platelet
310 activation, suggesting that MTA interacts with an unidentified G protein-coupled receptor that stimulates
311 cAMP production (40, 41).
312 The analysis of the negative ionization dataset revealed the enrichment of pyridine nucleotide cycling, L-
313 glutamine biosynthesis II (tRNA-dependent), asparagine biosynthesis I, arginine biosynthesis IV, NAD
314 biosynthesis from 2-amino-3-carboxymuconate semialdehyde and riboflavin, FMN and FAD
315 transformations pathways (NES score > 1.345, *p-value* < 0.05; Supplementary Table 4 and Figure 1B).
316 Interestingly, two main metabolites implicated in these pathways, AMP and FMN are deregulated.
317 Differential metabolite abundance analysis showed that NM1 KO Cells exhibit significantly higher levels
318 of AMP (*t* = 3.07, *p-value* = 0.015), and reduced levels of FMN (*t* = -3.43, *p* value = 0.009; Supplementary
319 Table 2 and 4, and Figure 1D). Elevated AMP and reduced FMN levels can significantly modulate platelet
320 activation through the interplay of cyclic AMP (cAMP) and phosphoinositide signaling pathways. cAMP
321 regulation is crucial, as it inhibits key processes in platelet activation, including calcium mobilization and
322 integrin activation, thereby reducing platelet aggregation and secretion (42, 43). Furthermore, increased
323 cAMP levels suppress G protein-mediated responses, leading to decreased thrombin-induced secretion
324 and aggregation (43). Reduced levels of FMN can disrupt calcium signaling, further influencing platelet
325 activation dynamics (44).

326 Altogether these observations suggest that loss of NM1 is associated with the differential abundance of
327 metabolites important for hemostasis and, in particular abundance of negative regulators of platelet
328 aggregation.
329
330 **NM1 deletion leads to deregulated expression of cytokines and proinflammatory chemokines**
331 Since platelet activation and aggregation play a role in modulating immune responses and
332 inflammation we next studied, if NM1 expression levels affect cytokines and proinflammatory chemokines
333 production using WT, NM1 KO, and rescued NM1 KO MEFs with exogenous NM1 expression (KO+NM1).
334 We measured the amounts of secreted cytokines and chemokines in growing media by using BioLegend
335 LEGENDplex bead-based immunoassays. The results show that most tested cytokines and chemokines
336 levels were altered in the NM1 KO background (Figure 1E and 1F). Except for IL-1β and IL-11, all other
337 cytokines tested including IL-1α, IL-3, IFN-β, IL-12p40, IL-23, IL-7, IL-33, GM-CSF, IL-12p70, IL-27, TSLP were
338 suppressed in the absence of NM1, with the majority being rescued by reintroducing exogenous NM1 in
339 the KO background (KO+NM1) (Figure 1E). Several chemokines show the same profile and their secretion
340 to media is suppressed in KO cells and restored in KO+NM1 cells (RANTES, Eotaxin, MCP-1, MIP-1β, BLC).
341 Only two chemokines show opposite effects in expression and are increased in NM1 knock-out cells (MIP-
342 3α, KC). The chemokines IP-10, MIP-1α and LIX do not show any change upon deletion of NM1 but their
343 expression is increased by the reintroduction of NM1 in the KO background, and chemokines TARC and
344 MDC are suppressed in KO cells but overexpression of NM1 did not lead to restoration of their levels
345 (Figure 1F). These cytokines and chemokines are essential for the proliferation and differentiation of
346 various hematopoietic cells contributing to immune cell development and inflammation processes.
347 Therefore, their broad deregulation in NM1 KO cells suggests the direct involvement of NM1 in the
348 development and functionality of immune system processes. As cytokines and chemokines are secreted
349 by many cell types and serve as broad signaling molecules, we wanted to test whether profiles observed

350 in NM1 knockout cells are specific to NM1 protein or whether their profile changes regardless of the
351 mutated gene. To test this, we used cells lacking beta-actin that exhibit pleiotropic effects on
352 transcription, chromatin remodeling, DNA damage response, and mitochondrial function similar to NM1
353 protein. We measured cytokines and chemokines produced by these cells and cells and compared them
354 to wild-type control cells. In comparison to NM1 deletion, the deletion of beta-actin has only a marginal
355 effect on cytokine production with only IL-1α being upregulated and GM-CSF being downregulated in
356 beta-actin knock-out cells (Supplementary Figure 1E). In contrast, the expression of several chemokines is
357 changed in beta-actin knockout cells (RANTES, TARC, KC, IP-10, and BLC are suppressed and MIP-3α, MCP-
358 1, MIP-1α, and LIX are upregulated) (Supplementary Figure 1F), however, these changes do not correlate
359 with data observed in NM1 KO cells, supporting a specific role of NM1 in the production of cytokines and
360 chemokines that might act as signaling molecules during hematopoiesis crosslinking platelets activation
361 signaling and immune responses.

362

363 **NM1 deletion affects the transcriptomic profile of hematopoietic tissues**

364 To find out if NM1 plays a role in regulating hematopoiesis in vivo, we next isolated RNA from
365 bone marrow, spleen, and peripheral blood from WT and NM1 KO mice for deep sequencing. Principal
366 Component Analysis (PCA) for each tissue shows that there is significant differential gene expression
367 between WT and KO conditions. Moreover, while WT samples show relatively high consistency between
368 the replicates, NMI KO tissue samples show higher variability suggesting that NM1 deletion leads to a
369 general imbalance in global gene expression in the selected tissues (Figure 2A). Due to high variability
370 between NM1 KO replicates, the total number of statistically significant differentially expressed genes is
371 lower in comparison to previously published RNA sequencing data from stable cell lines (7, 8). In bone
372 marrow tissue, there is an equal number of significantly up-regulated (374 genes) and significantly down-
373 regulated genes (358 genes). In the spleen, the majority of differentially expressed genes are

374 downregulated (1134 genes) and only 367 genes are upregulated. On the contrary, in blood, there are
375 248 upregulated genes and only 52 downregulated genes (Figure 2B). We next compared all differentially
376 expressed genes between the tissues to uncover whether the same set of genes is affected between
377 tissues (Figure 2C). The Venn diagram shows that the majority of differentially expressed genes are specific
378 for each tissue with only a minor part being shared between the groups. However, the shared genes show
379 a high degree of similarity in expression patterns between bone marrow and blood samples (Figure 2D),
380 moderate similarity between bone marrow and spleen samples (Figure 2E), and no similarity between
381 spleen and blood samples (Figure 2F).

382 This suggests that certain phenotypic changes upon NM1 deletion persist from early
383 hematopoiesis in the bone marrow to differentiated cell types in peripheral blood, while some others are
384 affected by the local environment and/or metabolic requirements of a given cell type.

385

386 **NM1 regulates hemostasis and platelet activation in mice**

387 Following RNAseq analysis, we first performed gene ontology analysis of all differentially
388 expressed genes to assess the biological processes and pathways specifically affected by NM1 deletion in
389 bone marrow, where hematopoietic differentiation occurs (Figure 3A). Among the most affected ones,
390 we found biological processes associated with extracellular matrix and cell adhesion, immune system
391 processes, platelet activation and coagulation, osteoclast differentiation, and regulation of PI3K-AKT,
392 Protein kinase B (PKB), MAPK-ERK or Rap1 signaling pathways. To identify the processes activated or
393 suppressed following NM1 deletion, we performed gene ontology analysis with only up-regulated (Figure
394 3B) or down-regulated genes (Figure 3C). While the majority of aforementioned processes are activated
395 upon NM1 deletion, osteoclast differentiation and processes related to the immune system and immune
396 response are suppressed in NM1 KO mice. This suggests that depending on the process, NM1 may have
397 an antagonistic effect on the expression of specific genes. All affected pathways have been shown to

398 regulate hematopoiesis stem cell maintenance and lineage development. PI3K-AKT signaling is a pro-
399 survival and pro-proliferative pathway that together with PKB signaling regulates the proliferation and
400 renewal of HSCs, and contributes to their differentiation. If deregulated, PI3K-AKT signaling dramatically
401 affects hematopoiesis leading to various hematologic malignancies (45-47). Rap1 signaling pathway
402 regulates extracellular matrix formation and cell adhesion and it is important for the differentiation of
403 megakaryocytes and platelets via MAPK-ERK pathways (48-50), which is in agreement with observed gene
404 ontology terms found in the upregulated genes related to the extracellular matrix, cell adhesion, and
405 platelet activation (Figure 3B).

406 Next, we focused on differentially expressed genes associated with hemopoietic differentiation,
407 platelet activation, and blood coagulation and performed STRING analysis of these genes to produce a
408 gene interaction map based on text mixing, experimental data, co-expression, and database search (36)
409 (Figure 4A). This analysis led to the discovery of two main clusters – genes directly involved in platelet
410 activation and blood coagulation processes (Cluster I), and genes involved in cell signaling cascades
411 (Cluster II). The first group contains collagen genes (Col1a1, Col1a2), which are recognized by von
412 Willbrand factor (Vwf), and genes expressing platelet glycoproteins (GP5, GP9, Gp1ba, GP1bb) which
413 attach platelets to collagen network directly or via Vwf. Integrins (Itgb3, Itga2b, Itgb1, Itga6) present on
414 the platelet plasma membrane then mediate platelet aggregation via binding to extracellular proteins
415 such as fibrinogen to form blood clots (51). Several other factors regulate platelet activation, including
416 platelet factor 4 (Pf4) released during platelet aggregation to neutralize the anticoagulant effect of
417 heparin, Multimerin 1 (Mmrn1) which stabilizes factor V in platelets, and the CD9 antigen (Cd9) that
418 controls platelet activation and aggregation via cell adhesion and others (Serpine2, Serping1, Thbd, Tfpi,
419 G6b, F2Rl3, F2Rl2, Pros1). The second group of genes identified in the STRING analysis is related to
420 different cellular signaling cascades having a role during cell adhesion, growth, and proliferation. This
421 group contains genes expressing Tyrosine-protein kinases (Mapk13, Mapk3, Src, Mertk), thyrosine-

422 protein phosphatases (Ptprj), receptors and ligands for thyrosine kinases (Kitl, Axl, Gas6), and G-protein
423 coupled signaling proteins (Adyc6, Adyc5, Il1A, Gnas, P2Ry1, Gucy1a3, Gucy1b3). The expression profile
424 of all differentially expressed genes across experimental samples associated with GO terms "Platelet
425 activation", "Hematopoietic cell lineage", and "Blood coagulation" is shown as a heatmap in descending
426 order (Figure 4B).

427 Since platelet activation is a key component of the complex response to vascular injury in
428 peripheral tissues, we next performed transcriptional profiling of WT and NM1 KO peripheral blood, the
429 site of action for circulating blood cells. We found a relatively low number of differentially expressed genes
430 (~300) with the majority of them being upregulated. Similarly to bone marrow, gene ontology analysis
431 shows the majority of upregulated GO terms are associated with blood coagulation, platelet activation,
432 hemostasis, and related processes such as rearrangement of the actin cytoskeleton, cell-matrix adhesion,
433 and integrin-mediated signaling of all differentially expressed genes (Supplementary Figure 2A and 2B).
434 We next plotted all genes associated with GO terms "Blood coagulation" and "Platelet activation" as
435 heatmaps in descending order (Supplementary Figure 2C and 2D respectively). We found several platelet
436 activation and coagulation genes (Vwf, F2rl2, Serpine2, Pros1, G6b), platelet glycoproteins (Gp1bb, Gp5,
437 Gp9, Gp1ba, Gp1bb), integrins (Itga2b, Itgb3, Itgb1) to be upregulated in NM1 KO blood samples as well
438 as in bone marrow. Above that, other platelet glycoproteins (Gp6), coagulation factors (F5, F10, F13a),
439 platelet activation and adhesion genes (Ptgs1, Fermt3, Anxa5), signaling proteins (Rasgrp2, Rap1b,
440 Rasgrp1), cytoskeletal proteins (Actb, Actg1, Mylk) and others to be specifically changed in NM1 KO blood
441 samples (Supplementary Figure 2C and 2D).

442 Next, we assessed the impact of NM1 deficiency on primary hemostasis, by measuring bleeding
443 time in WT and NM1 KO mice (Figure 5A). Surprisingly, even though NM1 deletion leads to hyperactivation
444 of platelet activation cascade, NM1 KO mice show significantly prolonged bleeding time in comparison to
445 WT ($p = 0.0326$), indicating a general impairment of clotting efficiency in the absence of NM1. The mean

446 bleeding time was 225.0 ± 35.18 sec in WT mice, whereas NM1 KO mice exhibited a significantly increased
447 mean bleeding time of 322.5 ± 101.1 sec (Figure 5B and Supplementary Figure 3). To investigate whether
448 in the NM1 KO condition platelet homeostasis is also affected, we next performed a complete blood count
449 (CBC) analysis in WT and KO mice. Given the prolonged bleeding time observed in KO mice, we aimed to
450 determine whether altered platelet numbers could contribute to impaired hemostasis. CBC analysis
451 revealed a significant reduction in platelet counts in KO mice compared to WT controls ($p = 0.05$). The
452 mean platelet count in WT mice was 174.7 ± 48.79 $\times 10^3/\mu L$, whereas KO mice exhibited a markedly lower
453 mean platelet count of 52.25 ± 26.85 $\times 10^3/\mu L$ (Figure 5B). In contrast to white blood cell (WBC) counts
454 which were not significantly different between the groups (Figure 5B and Supplementary Figure 3), CBC
455 analysis also revealed a significant drop in red blood cell (RBC) count (Figure 5B), a decrease in hematocrit
456 (HCT) levels and an increase in the average size of red blood cells (MCV) (see Supplementary figure 3) as
457 previously published (29).

458 Taken together, the observations from the metabolomics analysis of primary cells, RNA
459 sequencing of hematopoietic tissues, and functional assays point towards the complex role of NM1 in the
460 process of hemostasis with major effect on platelet differentiation and activation.

461

462 **NM1 regulates innate and adaptive immune cell differentiation and activation**

463 Following the results from cytokine and chemokine measurements in model cell lines and the
464 abundance of GO terms associated with the immune system in bone marrow, we next performed a String
465 analysis of genes related to the gene ontology term "Immune response process" (Figure 4C). We found
466 that they cluster into three distinguished groups. The first group of genes (Cluster I) is associated with the
467 innate immune system and defense response to viruses correlating with GO terms found in the gene
468 ontology analysis of downregulated genes in NM1 KO mice. Among them, we found the interferon

469 regulatory factor 7 (Ifn7), a key transcriptional regulator of type I interferon-dependent immune
470 responses against DNA and RNA viruses. Compatible with the identification of Ifn7, in the same group we
471 found the mitochondrial antiviral signaling protein (Mavs), a central factor in signal transduction upon
472 viral infection, required for activation of transcription factors regulating interferon beta expression (52).
473 Ifitm1 and Iftm3, interferon-induced transmembrane antiviral proteins which inhibit the entry of the
474 viruses to the host cell cytoplasm, also cluster in the same group, similarly to Serine incorporator 5
475 (Serinc5), required to restrict incorporation of viral particles into cells. We also found interferon-induced
476 genes such as Oas2 and Oas3, coding for 2'-5' oligoadenylatesynthetases 2 and 3, which are dsRNA-
477 activated antiviral enzymes that degrade viral RNA (53) and Samhd1 a cellular nuclease with dNTPase
478 activity that reduces cellular dNTP levels to protect cells from retroviral reverse transcription during viral
479 replication as well as Z-DNA-binding protein 1 (Zbp1), a cytoplasmic DNA sensor that detects DNA of viral
480 or bacterial origin. Finally, we identified Nlprp1a and Nlprp1b, two factors that play a crucial role in the
481 formation of the inflammasome in response to pathogens and other damage-associated signals.

482 In the second cluster (Cluster II) are proteins involved in intracellular signaling cascades and
483 immune regulatory proteins, some of which were already described in platelet activation (Src, Axl, Cd4).
484 In addition to those, we found hematopoietic tyrosine-protein kinase (Hck) which regulates phagocytosis
485 and neutrophil, monocyte, macrophage, and mast cell function during innate immune response. Protein
486 kinase C theta (Prkcq) regulates T-cell activation, proliferation, differentiation and survival. Tyrosine
487 protein-kinase Jak3 mediates essential signaling events in both innate and adaptive immunity and plays a
488 crucial role during T-cell development. The other immune system receptors and regulators found in these
489 clusters are TYRO protein tyrosine kinase-binding protein (Tyrobp), Tumor necrosis factor alpha-induced
490 protein 8-like protein 2 (Tnfaip8l2), leukocyte immunoglobulin-like receptor subfamily B member 3 (Pirb),
491 CMRF35-like molecule 5 (Cd300ld) and leukocyte specific transcript 1 (Lst1).

492 The third cluster of genes derived from the STRING analysis relates to the immune complement
493 system to enhance the phagocytosis and clearance of microbes and damaged cells. It contains
494 complement factors Cfd, C1s1, C1qc, C1rl and regulatory proteins Serping 1, which regulates the activation
495 of the complement system by inhibiting C1 factor (54) and Ficolin-1 (Fcna), which is extracellular lectin
496 functioning as a recognition receptor in innate immunity in the lectin complement system pathway (55).
497 Expression profile across biological replicates for all significantly different genes classified under GO term
498 "Immune system process" is shown as a heatmap in descending order (Figure 4D). As suggested by the
499 gene ontology analysis, the majority of genes related to the immune process is downregulated in NM1 KO
500 cells but the differences between the genotypes are less prominent in comparison to differential gene
501 expression related to platelet activation (Figure 4D).

502 Since many immune cells reside and get activated in secondary lymphoid organs, we next studied
503 potential changes in immunity pathways in spleen tissue isolated from NM1 WT and KO mice. Results
504 from gene ontology analysis show that the most significantly dysregulated biological processes and
505 pathways are associated with the cell cycle and cell division regulation, DNA replication, and chromosome
506 segregation, as well as immunoglobulin production and immunoglobulin-mediated immune response
507 (Figure 6A). To define which biological processes and pathways are positively or negatively affected by
508 NM1 deletion, we performed separate gene ontology analyses of only upregulated and only
509 downregulated genes in the NM1 KO spleen respectively. In contrast to bone marrow tissue, immune
510 system-related genes are predominantly upregulated in the NM1 KO spleen tissue (Figure 6B), and
511 downregulated genes are mostly associated with the cell cycle and cell division GO terms (Figure 6C). To
512 understand the differences in immune-related processes between the bone marrow and the spleen, we
513 took all differentially expressed genes listed under GO terms "immunoglobulin mediated immune
514 response", "immunoglobulin production", "immune response", "immune response process", "adaptive
515 immune response", "T-cell receptor signaling pathways", and "T cell activation" and performed the

516 STRING analysis of protein interactions. The majority of differentially expressed genes that could not be
517 mapped during the analysis are variable or constant gene segments of immunoglobulin heavy and light
518 chains that do not possess any particular function per se (Figure 7A). They are randomly combined by
519 V(D)J somatic recombination into functional heavy and light chains to produce variable antibodies. V(D)J
520 recombination is executed already during lymphoid development of B cells in bone marrow but antibodies
521 are presented only in mature naïve B cells present in the spleen and other tissues. Therefore, even though
522 this particular immunoglobulin gene expression profile is found in the spleen tissue, the phenotype itself
523 originates in the bone marrow. So, we looked at the expression profile of V(D)J recombination-specific
524 genes in bone marrow (Supplementary Table 5), and found Rag1 and Rag2 genes to be significantly
525 upregulated. These recombination-activating genes 1 and 2 initiate V(D)J recombination by introducing
526 double-strand breaks between the recombination signal sequence (RSS) and a coding segment of a
527 particular immunoglobulin heavy or light chain gene (56) and their overexpression leads to lymphocyte
528 malignancies and immunodeficiency (57-59). However, it is not known whether there is a direct link
529 between increased Rag1 and Rag 2 expression in the bone marrow and a particular combination of the
530 immunoglobulin heavy and light variable gene segments found in the NM1 KO spleen.

531 Next, we plotted all other immune-related genes into an interaction map based on the
532 experimental data, text mining, co-expression, and database search and divided them by their role in
533 innate (red) or adaptive (blue) immune systems (Figure 7B). The proteins marked by both colors have a
534 dual role in both types of immunity and proteins marked white are additional factors present in immune
535 cells without a direct link to either innate or adaptive immune systems. The only visible cluster of innate
536 immune genes is localized around Interferon regulatory factor 7 (Irf7) protein which is the master
537 regulator of type I-interferon genes and interferon-stimulated genes. The other proteins in the cluster are
538 different interferon-stimulated enzymes important for the innate immune response against viruses and
539 bacteria (Eif2ak2, Herc6, Oas3, Rsad2, Isg20, Serinc), and proteins activating proinflammatory NF-kappa-

540 B signaling (Ikbke, Traf4, Tifa). Other innate immune system-related genes are different regulatory and
541 signaling proteins (Riok3, Mfhas1, Ilrun, Zcchc3, Ccl8, Mst1r, F2rl1, Slamf7, Mcoln2), developmental and
542 differentiation genes (Akirin2, Tnfrsf14, Cd24a, Prdm1, Zap70, Jak3), and additional relevant genes.

543 Adaptive immune system-related genes (blue) form a big interconnected cluster of genes
544 regulating different aspects of T-cell and B-cell biology. To differentiate between them, we marked all
545 genes associated with B cells and T cells separately based on the 5 most significant GO terms associated
546 with each cell type (Supplementary figure 4A and 4B respectively) and found that the majority of
547 differentially expressed genes are associated with the T cell development and specification (Themis,
548 Foxp3, Prdm1, Fas, Jak3, Sema4a), cell surface receptors (Cd4, Cd8a, Cd8b1, Cd247) and T cell activation
549 and signaling (Itk, C3, Ctla4, Alcam, Slamf7, Irf4, Zap70, Tnfsrf14).

550 We then plotted all Innate immune system-related and adaptive immune system-related genes
551 into a heatmap in descending order based on their expression profile in the NM1 KO spleen (Figure 7C
552 and 7D). Interestingly, the majority of innate immune system genes are suppressed in the NM1 KO spleen
553 similarly to bone marrow, with some genes being shared between both tissues (Irf7, Endod1, Oas3) (Figure
554 7C). Many upregulated genes have a dual role in both types of immune response and are therefore
555 present also in the adaptive immune system heatmap. In contrast to the innate immune system, adaptive
556 immune system genes are mostly upregulated suggesting some antagonistic effect of NM1 on
557 differentiation and activation of both immune systems in mice. Interestingly, based on the expression
558 profile it seems that there is an overrepresentation of several types of regulatory T cells (Tregs). While
559 Cd4 and Cd8 are general markers of mature T cells, in combination with other factors define specific T-
560 cell subpopulations. Upregulated Foxp3 and Il2ra (CD25) are markers of Cd4+ Foxp3+ CD25+ (60), and
561 Cd8+ Foxp3+ CD25+ Treg cells (61). Upregulated Il2rb (CD122) is a marker of Cd8+ Cd122+ Treg cells which
562 are further specified by increased expression of Pdcd1 (Pd1) which is also upregulated (but not statistically

563 significant) in NM1 KO spleen (62-64) (Supplementary table 5). Ctla4 is upregulated in activated T-cells
564 but is also constitutively expressed in Cd8+ Ctla4+ Treg cells (65, 66) (Figure 7D).
565 We conclude that NM1 plays an important, possibly antagonistic role in innate and adaptive
566 immune systems. Given its effect on platelet differentiation and activation, we propose that NM1 plays a
567 general role in the communication and coordination of immune and hemostatic processes in mice.
568

569 **Discussion**

570 After the cell nucleus, mitochondria are probably the second most studied cellular organelle due
571 to their role as a powerhouse producing energy via oxidative phosphorylation in healthy cells. In contrast
572 to oxidative phosphorylation, aerobic glycolysis has long been considered a metabolic pathway typical of
573 cancer cells or a consequence of aberrant mitochondrial function. However, discoveries over the last
574 decade have shown that aerobic glycolysis is a full-featured pathway that does not only produce energy
575 but also provides specific byproducts and signaling molecules or specific intracellular and extracellular
576 conditions to many cell types. Moreover, there is a clear interplay between oxidative phosphorylation and
577 aerobic glycolysis and the energy production pathways can change even in the same cell type based on
578 the actual needs, cellular activity, or differentiation status. The regulation of this metabolic switch is still
579 poorly understood but it is getting gradual attention as it is associated with many metabolic disorders.
580 Recently, we discovered that NM1 plays a critical role in this process and its mutation or deletion leads to
581 a metabolic switch from oxidative phosphorylation to glycolysis, and subsequent tumorigenesis in mice
582 (8). Because of these observations, we hypothesized that NM1 may be a general factor regulating the
583 switch between oxidative phosphorylation and glycolysis in multiple tissues during the differentiation or
584 activation of specific cell types.
585 The bone marrow is a very heterogeneous tissue giving rise to several, mostly hematopoietic cell
586 types with very specific functions and metabolic needs, and thus it is an interesting non-cancerous model

587 to study whether NM1 depletion affects cell differentiation possibly by affecting the interplay between
588 oxidative phosphorylation and glycolysis. Several studies have suggested the involvement of both actin
589 and myosin in the regulation of the immune system (67). In addition, initial phenotyping of NM1 KO mice
590 as well as this study, revealed a decreased total number of red blood cells with higher corpuscular volume
591 and hemoglobin content and decreased bone mineral density suggesting that NM1 can play a role in the
592 differentiation of cells in bone marrow and other hematopoietic tissues (29). Therefore, we performed
593 transcriptomic analysis of the bone marrow, spleen, and peripheral blood isolated from NM1 WT and KO
594 mice to discover gene programs affected by NM1 deletion. Regarding decreased erythrocyte numbers
595 observed in NM1 KO mice, gene programs involved in erythrocyte differentiation are not significantly
596 affected. Although we have limited mechanistic insights at this stage, this result suggests that NM1 may
597 not have a specific role in erythrocyte differentiation or there are compensatory mechanisms upon NM1
598 deletion. Such mechanisms are observed in the so-called "sports anemia" when trained athletes have
599 decreased hematocrit but the total mass of red blood cells and hemoglobin levels are higher (68). The lack
600 of a dominant effect on transcription profiles during erythropoiesis could also be due to the very
601 metabolic setup of differentiated erythrocytes. Even though there is a short stage during differentiation
602 which depends on oxidative phosphorylation, final red blood cells fully depend on glycolysis (11). As NM1
603 deletion pushes cells toward glycolytic metabolism, erythrocytes should not be affected as much since
604 mature cells do not depend on oxidative phosphorylation. Similarly, osteoclasts which normally use
605 oxidative phosphorylation as the primary energy source and glycolysis only upon activation to increase
606 local acidosis (20), are transcriptionally suppressed in NM1 KO mice but NM1 KO mice have decreased
607 bone mineral density (29). Therefore, while differentiation of osteoclasts can be negatively affected by
608 NM1 loss, glycolysis-dependent bone resorption could be elevated in NM1 KO mice as seen in
609 osteoporotic patients with hyperactive osteoclasts with increased glycolysis and higher extracellular
610 acidity needed for bone resorption (20, 69).

611 The most affected pathways in the tested tissues were related to platelet activation and innate
612 and adaptive immune systems. Interestingly, even though the blood cell count shows a significantly lower
613 number of platelets in circulating blood and increased bleeding time in NM1 KO mice, the platelet
614 activation cascade was upregulated in the bone marrow and peripheral blood. Under normal conditions,
615 platelets are formed from proplatelet protrusions of megakaryocytes in the bone marrow. Upon their
616 release into the bloodstream, they are activated at the place of vessel wall injury leading to the
617 reorganization of their morphology and the formation of platelet plugs (70). Therefore, their decreased
618 number and hyperactivation already in the bone marrow suggest general deregulation of platelet
619 biogenesis in NM1 KO mice. We hypothesize that this is due to different metabolic requirements during
620 platelet differentiation and activation. Megakaryocytes depend on both glycolysis and OXPHOS for
621 energy, with glycolysis supporting early differentiation and polyploidization and later proplatelet
622 formation when ATP is needed for cytoskeletal remodeling and formation of the membrane protrusion
623 for platelet production (71). However, mitochondria-dependent reactive oxygen species production is
624 crucial for the initiation of thrombopoiesis, suggesting that functional OXPHOS plays a role in proplatelet
625 formation (72). Subsequently, circulating platelets depend again on both types of metabolism, but
626 glycolysis is required for their activation. Therefore, NM1 loss-dependent decrease in mitochondrial
627 OXPHOS metabolism could lead to decreased proplatelet formation in megakaryocytes and subsequent
628 reduction of circulating platelets, with glycolytic metabolism pushing them towards activation regardless
629 of the external stimuli. Proplatelet formation, followed by platelet segregation and platelet activation,
630 depends on the rearrangements of the actin cytoskeleton and plasma membrane. As NM1 directly links
631 the plasma membrane to the underlying cytoskeleton (4), phenotypes observed in platelets may arise not
632 only due to deregulated metabolism but also due faulty plasma membrane dynamics caused by NM1 loss.
633 Above the main role in blood coagulation, there is also increasing evidence of platelet
634 communication with immune cells in inflammation processes, osteoclast differentiation, and cancer

635 development and progression (73-76). This could be directly linked to phenotypes observed in innate and
636 adaptive immune responses. As mentioned before while innate immune system is suppressed in NM1 KO
637 mice, adaptive immune system and expression of specific sets of immunoglobulins are upregulated. While
638 this can be explained by metabolic reprogramming of given cells and a need for oxidative phosphorylation
639 for differentiation of innate immune monocytes or dendritic cells and glycolysis needed for activation of
640 B and T cells (12, 13). However, it is also plausible that NM1 affects the destiny of these cells differently.
641 Cell metabolism and, in general, proliferation are regulated by the PI3K/Akt/mTOR signaling pathway,
642 with mTOR activating the expression of many downstream targets. In particular, proliferation is heavily
643 regulated by this pathway, with mTOR activating the expression of many downstream targets, including
644 metabolic gene programs. We found that NM1 is a downstream target of mTOR to regulate the expression
645 of mitochondrial transcription factors, but it also regulates mTOR expression itself in a feedback loop.
646 Upon stimulation, mTOR activates NM1, which binds to the mTOR promoter and induces its expression as
647 long as the stimulus persists. Thus, deletion of NM1 may lead to suppression of mTOR signaling, while
648 another pathway may influence the processes observed in NM1 knockout mice. For example, a delicate
649 balance of the complex system of nutrient sensing and mTOR (mTORC1) signaling is crucial to ensure the
650 appropriate development of dendritic cells (77) The differentiation and survival of dendritic cells rely on
651 the mTOR complex 1 (mTORC1) activation and subsequent expression of the mTORC1 downstream target
652 peroxisomal proliferator-activated receptor γ (PPARγ) which affects cell maturation and function largely
653 through control of lipid metabolism and its function is abrogated by rapamycin, an mTOR/mTORC1
654 inhibitor (78-80). mTOR was also shown to have a role during the differentiation of B cells and VDJ
655 recombination. Here, the mutations in mTORC complex or treatment with rapamycin have positive
656 effects, and lead to enhanced pro-B cell survival, an increase in RAG1 and RAG2 recombinase expression,
657 and augmented V(D)J recombinase activity (81). As the same phenotypes can be observed in NM1 KO
658 immune cells, NM1 may regulate various aspects of hematopoiesis differentiation as a part of

659 PI3K/AKT/mTOR signaling via direct transcriptional regulation of their metabolism, or more broadly by
660 affecting some mTOR-dependent pathways.

661 Taken together, we showed that NM1 contributes to global body homeostasis by regulating the
662 differentiation and activity of specific hematopoietic cell types. We hypothesize that NM1 affects the
663 destiny of these cells by regulating their metabolism status, but the direct mechanism remains to be
664 elucidated and will be the objective of future studies.

665

666 **Acknowledgments**

667 This work was supported by grants from New York University Abu Dhabi, by Tamkeen under the NYU Abu
668 Dhabi Research Institute Award to the NYUAD Center for Genomics and Systems Biology (ADHPG-CGSB),
669 and by the Sheikh Hamdan Bin Rashid Al Maktoum Award for Medical Sciences to PP. We also
670 acknowledge the institutional support from the Institute of Molecular Genetics of the Czech Academy of
671 Sciences (RVO: 68378050) and the Research Program Strategy AV21 Future of Assisted Reproduction
672 (ART) (AV21-VP38/2025) provided by the Czech Agency of Sciences to TV and PH. RNA sequencing was
673 performed by the NYUAD CGSB Core at New York University Abu Dhabi and Bioinformatics assistance was
674 provided by the NYUAD Bioinformatics Core at New York University Abu Dhabi. We would like to thank
675 Marc Arnoux for assistance with deep sequencing and Nizar Drou for assistance with the analysis.

676

677 **Author Contributions**

678 TV designed and performed the majority of experiments, analyzed the sequencing data, and wrote the
679 manuscript together with PP. SK, VF, RS, performed functional assays in mice. WA and YI analyzed the
680 metabolomic data. MEG and JCMT performed cytokine assays. PH provided the NM1 KO mice and
681 contributed to manuscript writing. PP supervised the research project, wrote the manuscript, and
682 analyzed the data.

683

684 **Conflict of interest**

685 There is no conflict of interest.

686 **References**

687 1. Venit T, El Said NH, Mahmood SR, Percipalle P. A dynamic actin-dependent nucleoskeleton and
688 cell identity. J Biochem. 2021;169(3):243-57.
689 2. Venit T, Mahmood SR, Endara-Coll M, Percipalle P. Nuclear actin and myosin in chromatin
690 regulation and maintenance of genome integrity. Int Rev Cell Mol Biol. 2020;355:67-108.
691 3. Dzijak R, Yildirim S, Kahle M, Novak P, Hnilicova J, Venit T, et al. Specific nuclear localizing
692 sequence directs two myosin isoforms to the cell nucleus in calmodulin-sensitive manner. PLoS One.
693 2012;7(1):e30529.
694 4. Venit T, Kalendova A, Petr M, Dzijak R, Pastorek L, Rohozkova J, et al. Nuclear myosin I regulates
695 cell membrane tension. Sci Rep. 2016;6:30864.
696 5. Sarshad A, Sadeghifar F, Louvet E, Mori R, Bohm S, Al-Muzzaini B, et al. Nuclear myosin 1c
697 facilitates the chromatin modifications required to activate rRNA gene transcription and cell cycle
698 progression. PLoS Genet. 2013;9(3):e1003397.
699 6. Almuzzaini B, Sarshad AA, Farrants AK, Percipalle P. Nuclear myosin 1 contributes to a chromatin
700 landscape compatible with RNA polymerase II transcription activation. BMC Biol. 2015;13:35.
701 7. Venit T, Semesta K, Farrukh S, Endara-Coll M, Havalda R, Hozak P, et al. Nuclear myosin 1
702 activates p21 gene transcription in response to DNA damage through a chromatin-based mechanism.
703 Commun Biol. 2020;3(1):115.
704 8. Venit T, Sapkota O, Abdrabou WS, Loganathan P, Pasricha R, Mahmood SR, et al. Positive
705 regulation of oxidative phosphorylation by nuclear myosin 1 protects cells from metabolic
706 reprogramming and tumorigenesis in mice. Nat Commun. 2023;14(1):6328.
707 9. Yu VW, Scadden DT. Heterogeneity of the bone marrow niche. Curr Opin Hematol.
708 2016;23(4):331-8.

709 10. Morganti C, Cabezas-Wallscheid N, Ito K. Metabolic Regulation of Hematopoietic Stem Cells.
710 Hemasphere. 2022;6(7):e740.
711 11. Zhang ZW, Cheng J, Xu F, Chen YE, Du JB, Yuan M, et al. Red blood cell extrudes nucleus and
712 mitochondria against oxidative stress. IUBMB Life. 2011;63(7):560-5.
713 12. Shapiro H, Lutaty A, Ariel A. Macrophages, meta-inflammation, and immuno-metabolism.
714 ScientificWorldJournal. 2011;11:2509-29.
715 13. O'Neill LA, Hardie DG. Metabolism of inflammation limited by AMPK and pseudo-starvation.
716 Nature. 2013;493(7432):346-55.
717 14. Macintyre AN, Rathmell JC. Activated lymphocytes as a metabolic model for carcinogenesis.
718 Cancer Metab. 2013;1(1):5.
719 15. Jeon JH, Hong CW, Kim EY, Lee JM. Current Understanding on the Metabolism of Neutrophils.
720 Immune Netw. 2020;20(6):e46.
721 16. Kulkarni PP, Tiwari A, Singh N, Gautam D, Sonkar VK, Agarwal V, et al. Aerobic glycolysis fuels
722 platelet activation: small-molecule modulators of platelet metabolism as anti-thrombotic agents.
723 Haematologica. 2019;104(4):806-18.
724 17. Aibibula M, Naseem KM, Sturmey RG. Glucose metabolism and metabolic flexibility in blood
725 platelets. J Thromb Haemost. 2018;16(11):2300-14.
726 18. Palomaki S, Pietila M, Laitinen S, Pesala J, Sormunen R, Lehenkari P, et al. HIF-1alpha is
727 upregulated in human mesenchymal stem cells. Stem Cells. 2013;31(9):1902-9.
728 19. Lee WC, Guntur AR, Long F, Rosen CJ. Energy Metabolism of the Osteoblast: Implications for
729 Osteoporosis. Endocr Rev. 2017;38(3):255-66.
730 20. Ahn H, Lee K, Kim JM, Kwon SH, Lee SH, Lee SY, et al. Accelerated Lactate Dehydrogenase
731 Activity Potentiates Osteoclastogenesis via NFATc1 Signaling. PLoS One. 2016;11(4):e0153886.

732 21. Lemma S, Sboarina M, Porporato PE, Zini N, Sonveaux P, Di Pompo G, et al. Energy metabolism
733 in osteoclast formation and activity. Int J Biochem Cell Biol. 2016;79:168-80.
734 22. Mahmood SR, Xie X, Hosny El Said N, Venit T, Gunsalus KC, Percipalle P. beta-actin dependent
735 chromatin remodeling mediates compartment level changes in 3D genome architecture. Nat Commun.
736 2021;12(1):5240.
737 23. Xie X, Venit T, Drou N, Percipalle P. In Mitochondria ?-Actin Regulates mtDNA Transcription and
738 Is Required for Mitochondrial Quality Control. iScience. 2018;3:226-37.
739 24. Hackstadt AJ, Hess AM. Filtering for increased power for microarray data analysis. BMC
740 Bioinformatics. 2009;10:11.
741 25. Pang Z, Lu Y, Zhou G, Hui F, Xu L, Viau C, et al. MetaboAnalyst 6.0: towards a unified platform for
742 metabolomics data processing, analysis and interpretation. Nucleic Acids Res. 2024;52(W1):W398-
743 W406.
744 26. Caspi R, Foerster H, Fulcher CA, Kaipa P, Krummenacker M, Latendresse M, et al. The MetaCyc
745 Database of metabolic pathways and enzymes and the BioCyc collection of Pathway/Genome
746 Databases. Nucleic Acids Res. 2008;36(Database issue):D623-31.
747 27. Karp PD, Paley SM, Krummenacker M, Latendresse M, Dale JM, Lee TJ, et al. Pathway Tools
748 version 13.0: integrated software for pathway/genome informatics and systems biology. Brief Bioinform.
749 2010;11(1):40-79.
750 28. Lu Y, Pang Z, Xia J. Comprehensive investigation of pathway enrichment methods for functional
751 interpretation of LC-MS global metabolomics data. Brief Bioinform. 2023;24(1).
752 29. Venit T, Dzijak R, Kalendova A, Kahle M, Rohozkova J, Schmidt V, et al. Mouse nuclear myosin I
753 knock-out shows interchangeability and redundancy of myosin isoforms in the cell nucleus. PLoS One.
754 2013;8(4):e61406.

755 30. Amend SR, Valkenburg KC, Pienta KJ. Murine Hind Limb Long Bone Dissection and Bone Marrow
756 Isolation. J Vis Exp. 2016(110).
757 31. Golde WT, Gollobin P, Rodriguez LL. A rapid, simple, and humane method for submandibular
758 bleeding of mice using a lancet. Lab Anim (NY). 2005;34(9):39-43.
759 32. Bolger AM, Lohse M, Usadel B. Trimmomatic: a flexible trimmer for Illumina sequence data.
760 Bioinformatics. 2014;30(15):2114-20.
761 33. Kim D, Langmead B, Salzberg SL. HISAT: a fast spliced aligner with low memory requirements.
762 Nat Methods. 2015;12(4):357-60.
763 34. Li H, Handsaker B, Wysoker A, Fennell T, Ruan J, Homer N, et al. The Sequence Alignment/Map
764 format and SAMtools. Bioinformatics. 2009;25(16):2078-9.
765 35. Huang da W, Sherman BT, Lempicki RA. Systematic and integrative analysis of large gene lists
766 using DAVID bioinformatics resources. Nat Protoc. 2009;4(1):44-57.
767 36. Szklarczyk D, Gable AL, Nastou KC, Lyon D, Kirsch R, Pyysalo S, et al. The STRING database in
768 2021: customizable protein-protein networks, and functional characterization of user-uploaded
769 gene/measurement sets. Nucleic Acids Res. 2021;49(D1):D605-D12.
770 37. Mohammed BM, Monroe DM, Gailani D. Mouse models of hemostasis. Platelets.
771 2020;31(4):417-22.
772 38. Parveen N, Cornell KA. Methylthioadenosine/S-adenosylhomocysteine nucleosidase, a critical
773 enzyme for bacterial metabolism. Mol Microbiol. 2011;79(1):7-20.
774 39. Sekowska A, Ashida H, Danchin A. Revisiting the methionine salvage pathway and its paralogues.
775 Microb Biotechnol. 2019;12(1):77-97.
776 40. Fuentes E, Pereira J, Mezzano D, Alarcon M, Caballero J, Palomo I. Inhibition of platelet
777 activation and thrombus formation by adenosine and inosine: studies on their relative contribution and
778 molecular modeling. PLoS One. 2014;9(11):e112741.

779 41. Srinivasan S, Mir F, Huang JS, Khasawneh FT, Lam SC, Le Breton GC. The P2Y12 antagonists, 2-
780 methylthioadenosine 5'-monophosphate triethylammonium salt and cangrelor (ARC69931MX), can
781 inhibit human platelet aggregation through a Gi-independent increase in cAMP levels. J Biol Chem.
782 2009;284(24):16108-17.
783 42. Feijge MA, Ansink K, Vanschoonbeek K, Heemskerk JW. Control of platelet activation by cyclic
784 AMP turnover and cyclic nucleotide phosphodiesterase type-3. Biochem Pharmacol. 2004;67(8):1559-
785 67.
786 43. Ryningen A, Olav Jensen B, Holmsen H. Elevation of cyclic AMP decreases phosphoinositide
787 turnover and inhibits thrombin-induced secretion in human platelets. Biochim Biophys Acta.
788 1998;1394(2-3):235-48.
789 44. Kishi Y, Ashikaga T, Numano F. Alteration of adenine nucleotide metabolism in coronary smooth
790 muscle cells by activated platelets. Thromb Res. 1992;65(4-5):571-84.
791 45. Silva A, Yunes JA, Cardoso BA, Martins LR, Jotta PY, Abecasis M, et al. PTEN posttranslational
792 inactivation and hyperactivation of the PI3K/Akt pathway sustain primary T cell leukemia viability. J Clin
793 Invest. 2008;118(11):3762-74.
794 46. Ringshausen I, Schneller F, Bogner C, Hipp S, Duyster J, Peschel C, et al. Constitutively activated
795 phosphatidylinositol-3 kinase (PI-3K) is involved in the defect of apoptosis in B-CLL: association with
796 protein kinase Cdelta. Blood. 2002;100(10):3741-8.
797 47. Polak R, Buitenhuis M. The PI3K/PKB signaling module as key regulator of hematopoiesis:
798 implications for therapeutic strategies in leukemia. Blood. 2012;119(4):911-23.
799 48. Stork PJ, Dillon TJ. Multiple roles of Rap1 in hematopoietic cells: complementary versus
800 antagonistic functions. Blood. 2005;106(9):2952-61.
801 49. Geest CR, Coffer PJ. MAPK signaling pathways in the regulation of hematopoiesis. J Leukoc Biol.
802 2009;86(2):237-50.

803 50. Baumgartner C, Toifl S, Farlik M, Halbritter F, Scheicher R, Fischer I, et al. An ERK-Dependent
804 Feedback Mechanism Prevents Hematopoietic Stem Cell Exhaustion. Cell Stem Cell. 2018;22(6):879-92
805 e6.
806 51. Dwivedi R, Pomin VH. Marine Antithrombotics. Mar Drugs. 2020;18(10).
807 52. Ren Z, Ding T, Zuo Z, Xu Z, Deng J, Wei Z. Regulation of MAVS Expression and Signaling Function
808 in the Antiviral Innate Immune Response. Front Immunol. 2020;11:1030.
809 53. Choi UY, Kang JS, Hwang YS, Kim YJ. Oligoadenylate synthase-like (OASL) proteins: dual functions
810 and associations with diseases. Exp Mol Med. 2015;47(3):e144.
811 54. Gorelik A, Sapir T, Woodruff TM, Reiner O. Serping1/C1 Inhibitor Affects Cortical Development in
812 a Cell Autonomous and Non-cell Autonomous Manner. Front Cell Neurosci. 2017;11:169.
813 55. Matsushita M, Kuraya M, Hamasaki N, Tsujimura M, Shiraki H, Fujita T. Activation of the lectin
814 complement pathway by H-ficolin (Hakata antigen). J Immunol. 2002;168(7):3502-6.
815 56. Akamatsu Y, Oettinger MA. Distinct roles of RAG1 and RAG2 in binding the V(D)J recombination
816 signal sequences. Mol Cell Biol. 1998;18(8):4670-8.
817 57. Miyazaki K, Miyazaki M. The Interplay Between Chromatin Architecture and Lineage-Specific
818 Transcription Factors and the Regulation of Rag Gene Expression. Front Immunol. 2021;12:659761.
819 58. Nussenzweig A, Nussenzweig MC. Origin of chromosomal translocations in lymphoid cancer.
820 Cell. 2010;141(1):27-38.
821 59. Rommel PC, Oliveira TY, Nussenzweig MC, Robbiani DF. RAG1/2 induces genomic insertions by
822 mobilizing DNA into RAG1/2-independent breaks. J Exp Med. 2017;214(3):815-31.
823 60. Chatenoud L. Natural and induced T CD4+CD25+FOXP3+ regulatory T cells. Methods Mol Biol.
824 2011;677:3-13.

825 61. Churlaud G, Pitoiset F, Jebbawi F, Lorenzon R, Bellier B, Rosenzwajg M, et al. Human and Mouse
826 CD8(+)CD25(+)FOXP3(+) Regulatory T Cells at Steady State and during Interleukin-2 Therapy. Front
827 Immunol. 2015;6:171.
828 62. Dai H, Wan N, Zhang S, Moore Y, Wan F, Dai Z. Cutting edge: programmed death-1 defines
829 CD8+CD122+ T cells as regulatory versus memory T cells. J Immunol. 2010;185(2):803-7.
830 63. Li S, Xie Q, Zeng Y, Zou C, Liu X, Wu S, et al. A naturally occurring CD8(+)CD122(+) T-cell subset as
831 a memory-like Treg family. Cell Mol Immunol. 2014;11(4):326-31.
832 64. Wang LX, Li Y, Yang G, Pang PY, Haley D, Walker EB, et al. CD122+CD8+ Treg suppress vaccine-
833 induced antitumor immune responses in lymphodepleted mice. Eur J Immunol. 2010;40(5):1375-85.
834 65. Olson BM, Jankowska-Gan E, Becker JT, Vignali DA, Burlingham WJ, McNeel DG. Human prostate
835 tumor antigen-specific CD8+ regulatory T cells are inhibited by CTLA-4 or IL-35 blockade. J Immunol.
836 2012;189(12):5590-601.
837 66. Vieyra-Lobato MR, Vela-Ojeda J, Montiel-Cervantes L, Lopez-Santiago R, Moreno-Lafont MC.
838 Description of CD8(+) Regulatory T Lymphocytes and Their Specific Intervention in Graft-versus-Host and
839 Infectious Diseases, Autoimmunity, and Cancer. J Immunol Res. 2018;2018:3758713.
840 67. Record J, Saeed MB, Venit T, Percipalle P, Westerberg LS. Journey to the Center of the Cell:
841 Cytoplasmic and Nuclear Actin in Immune Cell Functions. Front Cell Dev Biol. 2021;9:682294.
842 68. Mairbaurl H. Red blood cells in sports: effects of exercise and training on oxygen supply by red
843 blood cells. Front Physiol. 2013;4:332.
844 69. Xue L, Jiang Y, Han T, Zhang N, Qin L, Xin H, et al. Comparative proteomic and metabolomic
845 analysis reveal the antiosteoporotic molecular mechanism of icariin from Epimedium brevicornu maxim.
846 J Ethnopharmacol. 2016;192:370-81.
847 70. Luu S, Gardiner EE, Andrews RK. Bone Marrow Defects and Platelet Function: A Focus on MDS
848 and CLL. Cancers (Basel). 2018;10(5).

849 71. Handagama PJ, Feldman BF, Jain NC, Farver TB, Kono CS. In vitro platelet release by rat
850 megakaryocytes: effect of metabolic inhibitors and cytoskeletal disrupting agents. Am J Vet Res.
851 1987;48(7):1142-6.
852 72. Poirault-Chassac S, Nivet-Antoine V, Houvert A, Kauskot A, Lauret E, Lai-Kuen R, et al.
853 Mitochondrial dynamics and reactive oxygen species initiate thrombopoiesis from mature
854 megakaryocytes. Blood Adv. 2021;5(6):1706-18.
855 73. Maitz P, Kandler B, Fischer MB, Watzek G, Gruber R. Activated platelets retain their potential to
856 induce osteoclast-like cell formation in murine bone marrow cultures. Platelets. 2006;17(7):477-83.
857 74. Stoiber D, Assinger A. Platelet-Leukocyte Interplay in Cancer Development and Progression.
858 Cells. 2020;9(4).
859 75. Totani L, Evangelista V. Platelet-leukocyte interactions in cardiovascular disease and beyond.
860 Arterioscler Thromb Vasc Biol. 2010;30(12):2357-61.
861 76. Madel MB, Ibanez L, Wakkach A, de Vries TJ, Teti A, Apparailly F, et al. Immune Function and
862 Diversity of Osteoclasts in Normal and Pathological Conditions. Front Immunol. 2019;10:1408.
863 77. Sukhbaatar N, Hengstschlager M, Weichhart T. mTOR-Mediated Regulation of Dendritic Cell
864 Differentiation and Function. Trends Immunol. 2016;37(11):778-89.
865 78. Gogolak P, Rethi B, Szatmari I, Lanyi A, Dezso B, Nagy L, et al. Differentiation of CD1a- and CD1a+
866 monocyte-derived dendritic cells is biased by lipid environment and PPARgamma. Blood.
867 2007;109(2):643-52.
868 79. Haidinger M, Poglitsch M, Geyeregger R, Kasturi S, Zeyda M, Zlabinger GJ, et al. A versatile role
869 of mammalian target of rapamycin in human dendritic cell function and differentiation. J Immunol.
870 2010;185(7):3919-31.
871 80. Szatmari I, Torocsik D, Agostini M, Nagy T, Gurnell M, Barta E, et al. PPARgamma regulates the
872 function of human dendritic cells primarily by altering lipid metabolism. Blood. 2007;110(9):3271-80.

873 81. Lazorchak AS, Liu D, Facchinetti V, Di Lorenzo A, Sessa WC, Schatz DG, et al. Sin1-mTORC2
874 suppresses rag and il7r gene expression through Akt2 in B cells. Mol Cell. 2010;39(3):433-43.

875

876 Supplementary information is available on CMI's website.

877

878

879

880

881

882

883

884

885

886

887

888

889

890

891

892 **Figure legends**

893 **Figure 1. NM1 deletion leads to changes in hematopoietic signature metabolites and**
894 **cytokine/chemokine production in mouse embryonic fibroblasts. (a)** Gene Set Enrichment Analysis
895 (GSEA) for metabolic features detected using positive ionization. **(b)** Gene Set Enrichment Analysis (GSEA)
896 for metabolic features detected using negative ionization. **(c)** Metabolomic profile of 5-
897 methylthioadenosine (MTA) across experimental samples as detected by positive ionization. *** P≤0.001
898 **(d)** Metabolomic profile of AMP and FMN across experimental samples as detected by negative ionization.
899 * P≤0.05, *** P≤0.001 **(e)** List of analyzed cytokines in NM1 WT, NM1 KO and rescued NM1 KO+NM1 cells.
900 ns P > 0.05, * P≤0.05, ** P≤0.001, *** P≤0.001, **** P≤0.0001. **(f)** List of analyzed chemokines in NM1
901 WT, NM1 KO, and rescued NM1 KO+NM1 cells. ns P > 0.05, * P≤0.05, ** P≤0.001, *** P≤0.001, ****
902 P≤0.0001.

903 **Figure 2. NM1 deletion affects the transcriptomic profile of hematopoietic tissues. (a)** PCA plot showing
904 the distribution of RNA-seq samples isolated from NM1 WT and KO bone marrow, spleen, and blood
905 samples. **(b)** MA plot visualization of the differences in gene expression between experimental conditions
906 as a function of log fold change versus the mean of normalized counts. Each dot represents a single gene
907 expression profile with only red-marked genes to be significantly differentially expressed. **(c)** Venn
908 diagram showing the intersection in all differentially expressed genes between hematopoietic tissues. **(d)**
909 Expression heatmap of all differentially expressed genes shared between bone marrow and blood samples
910 organized in descending order. **(e)** Expression heatmap of all differentially expressed genes shared
911 between bone marrow and spleen samples organized in descending order. **(f)** Expression heatmap of all
912 differentially expressed genes shared between spleen and blood samples organized in descending order.

913 **Figure 3. Gene ontology analysis of bone marrow samples isolated from NM1 WT and KO mice. (a)** Gene
914 ontology analysis based on all differentially expressed genes between experimental conditions shows
915 biological process-, cellular component-, and KEGG pathway-associated gene ontology terms plotted in

916 descending order based on their significance. **(b)** Gene ontology analysis based on only upregulated genes
917 in NM1 KO samples. **(c)** Gene ontology analysis based on only downregulated genes in NM1 KO samples.

918 **Figure 4. Gene expression analysis of genes associated with platelet activation and immune system**
919 **process in the bone marrow. (a)** String analysis diagram of all genes associated with a KEGG GO term
920 "Platelet activation", a Biological process GO term "Platelet activation", KEGG GO term "Haemopoietic
921 cell lineage", and Biological GO term "Blood coagulation". **(b)** Heatmap of all differentially expressed
922 genes between NM1 WT and KO bone marrow samples associated with Platelet activation GO terms used
923 in String analysis. **(c)** String analysis diagram of all genes associated with GO term "Innate immune
924 system". **(d)** Heatmap of all differentially expressed genes between NM1 WT and KO bone marrow
925 samples associated with Innate immune system GO term used for the String analysis.

926 **Figure 5. NM1 deficiency leads to prolonged bleeding time and decreased number of platelets. (a)**
927 Schematic diagram illustrating the experimental procedure, where mice undergo tail cut for bleeding time
928 (BT) measurement. Following this, whole blood is collected via cardiac puncture for subsequent CBC
929 analysis. **(b)** Bar graph (Mean±SD) showing bleeding time (BT) between WT and NM1 KO mice (n = 5 WT,
930 9 KO). Additional violin plots show PTL, WBC, and RBC for both groups (n = 3 WT, 4 KO). The two-tailed
931 Mann-Whitney U test was used for statistical analysis. * $P \leq 0.05$, ** $P \leq 0.001$, *** $P \leq 0.001$, **** $P \leq 0.0001$.

932 **Figure 6. Gene ontology analysis of spleen isolated from NM1 WT and KO mice. (a)** Gene ontology
933 analysis based on all differentially expressed genes between experimental conditions shows biological
934 process-, cellular component-, and KEGG pathway-associated gene ontology terms plotted in descending
935 order based on their significance. **(b)** Gene ontology analysis based on only upregulated genes in NM1 KO
936 samples. **(c)** Gene ontology analysis based on only downregulated genes in NM1 KO samples.

937 **Figure 7. Gene expression analysis of genes associated with the innate and adaptive immune system in**
938 **the spleen. (a)** Heatmap of all differentially expressed genes between NM1 WT and KO spleen samples

939 associated with Immunoglobulin production which could not be mapped in String analysis **(b)** String
940 analysis diagram of all genes associated with GO term "Immune system". Genes marker red are associated
941 with the innate immune system while genes marked blue are associated with adaptive immune system.
942 **(c)** Heatmap of all differentially expressed genes between NM1 WT and KO spleen samples associated
943 with the innate immune system. **(d)** Heatmap of all differentially expressed genes between NM1 WT and
944 KO spleen samples associated with the adaptive immune system.

945

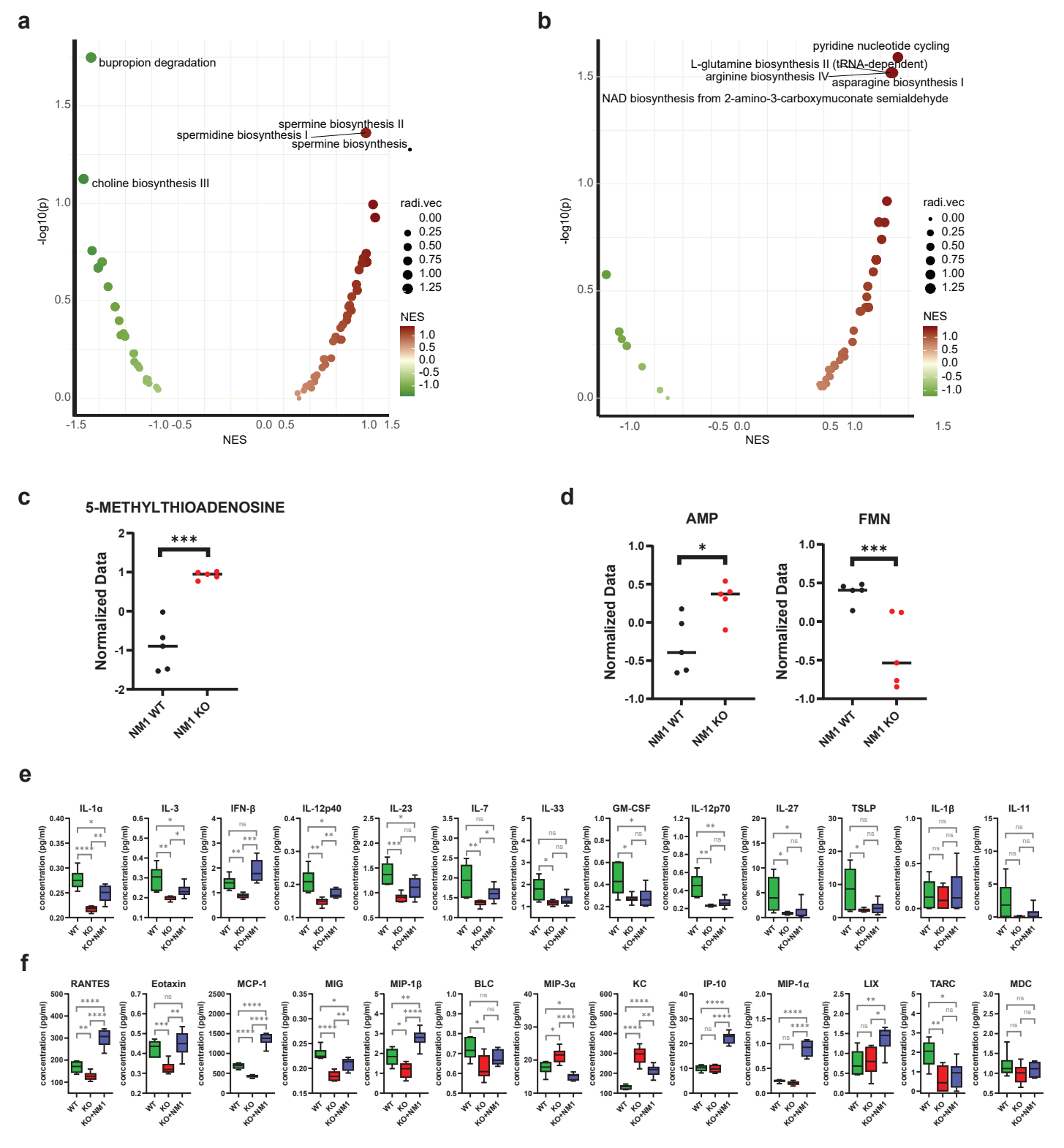
a
bupropion degradation
spermine biosynthesis II
spermidine biosynthesis I
spermine biosynthesis
choline biosynthesis III
-log10(p)
NES
radi.vec
0.00
0.25
0.50
0.75
1.00
1.25
b
pyridine nucleotide cycling
L-glutamine biosynthesis II (tRNA-dependent)
arginine biosynthesis IV
asparagine biosynthesis I
NAD biosynthesis from 2-amino-3-carboxymuconate semialdehyde
c
5-METHYLTHIOADENOSINE
Normalized Data
NM1 WT
NM1 KO
d
AMP
FMN
e
IL-1α
IL-3
IFN-β
IL-12p40
IL-23
IL-7
IL-33
GM-CSF
IL-12p70
IL-27
TSLP
IL-1β
IL-11
concentration (pg/ml)
WT
KO
KO+NM1
f
RANTES
Eotaxin
MCP-1
MIG
MIP-1β
BLC
MIP-3α
KC
IP-10
MIP-1α
LIX
TARC
MDC

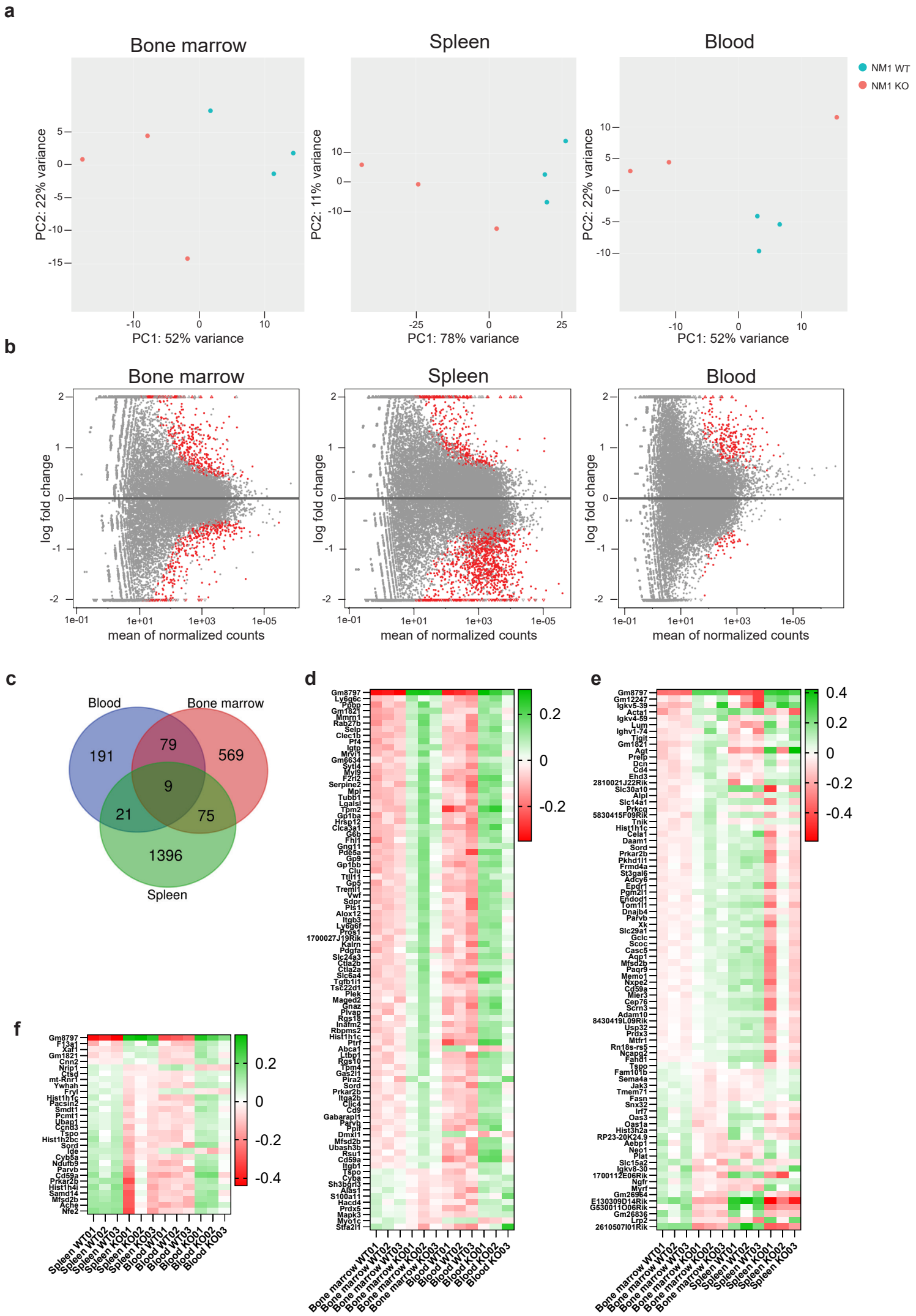
a
Bone marrow
Spleen
Blood
NM1 WT
NM1 KO
PC2: 22% variance
PC1: 52% variance
PC2: 11% variance
PC1: 78% variance
b
log fold change
mean of normalized counts
c
Blood
Bone marrow
Spleen
191
79
569
9
21
75
1396
d
e
f

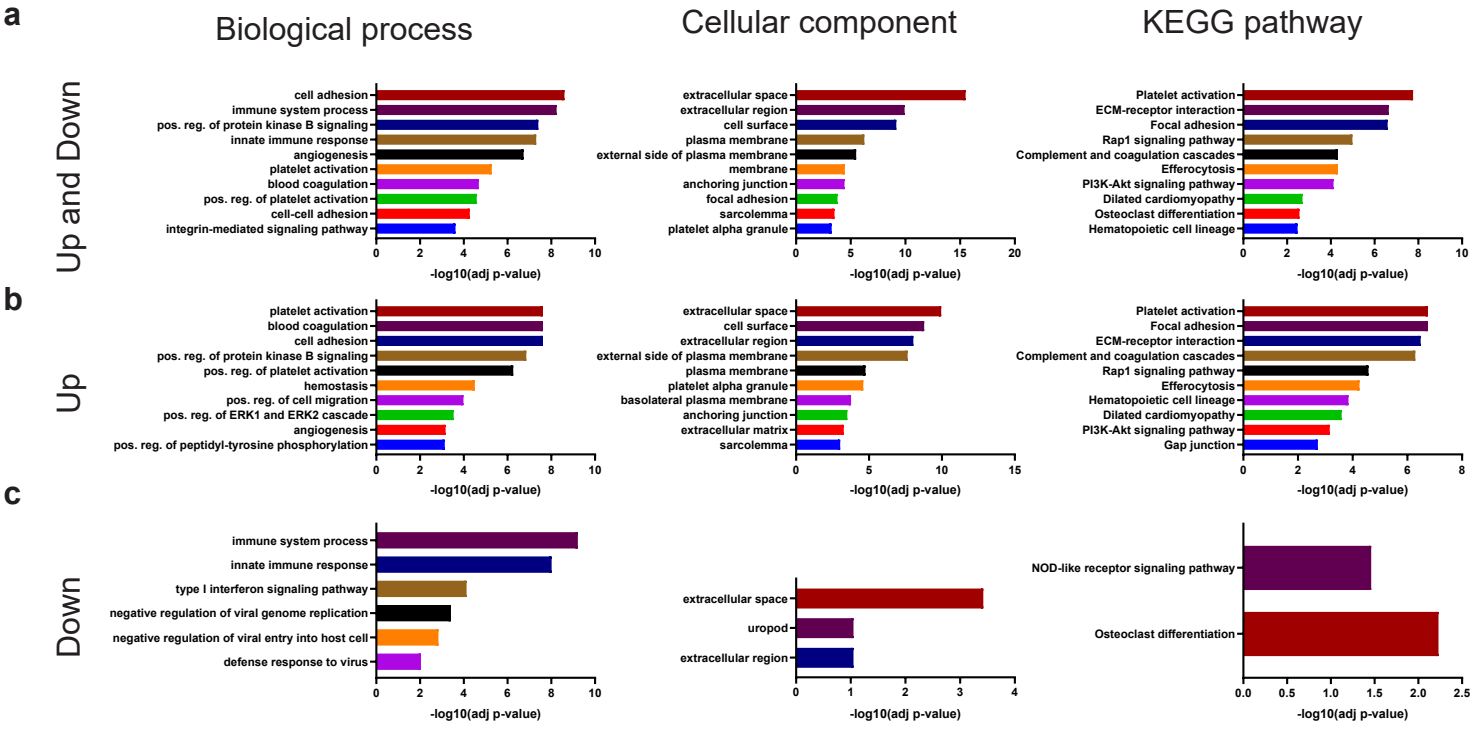
a
Biological process
Cellular component
KEGG pathway
Up and Down
cell adhesion
immune system process
pos. reg. of protein kinase B signaling
innate immune response
angiogenesis
platelet activation
blood coagulation
pos. reg. of platelet activation
cell-cell adhesion
integrin-mediated signaling pathway
0 2 4 6 8 10
-log10(adj p-value)
extracellular space
extracellular region
cell surface
plasma membrane
external side of plasma membrane
membrane
anchoring junction
focal adhesion
sarcolemma
platelet alpha granule
0 5 10 15 20
-log10(adj p-value)
Platelet activation
ECM-receptor interaction
Focal adhesion
Rap1 signaling pathway
Complement and coagulation cascades
Efferocytosis
PI3K-Akt signaling pathway
Dilated cardiomyopathy
Osteoclast differentiation
Hematopoietic cell lineage
0 2 4 6 8 10
-log10(adj p-value)
b
Up
platelet activation
blood coagulation
cell adhesion
pos. reg. of protein kinase B signaling
pos. reg. of platelet activation
hemostasis
pos. reg. of cell migration
pos. reg. of ERK1 and ERK2 cascade
angiogenesis
pos. reg. of peptidyl-tyrosine phosphorylation
0 2 4 6 8 10
-log10(adj p-value)
extracellular space
cell surface
extracellular region
external side of plasma membrane
plasma membrane
platelet alpha granule
basolateral plasma membrane
anchoring junction
extracellular matrix
sarcolemma
0 5 10 15
-log10(adj p-value)
Platelet activation
Focal adhesion
ECM-receptor interaction
Complement and coagulation cascades
Rap1 signaling pathway
Efferocytosis
Hematopoietic cell lineage
Dilated cardiomyopathy
PI3K-Akt signaling pathway
Gap junction
0 2 4 6 8
-log10(adj p-value)
c
Down
immune system process
innate immune response
type I interferon signaling pathway
negative regulation of viral genome replication
negative regulation of viral entry into host cell
defense response to virus
0 2 4 6 8 10
-log10(adj p-value)
extracellular space
uropod
extracellular region
0 1 2 3 4
-log10(adj p-value)
NOD-like receptor signaling pathway
Osteoclast differentiation
0.0 0.5 1.0 1.5 2.0 2.5
-log10(adj p-value)

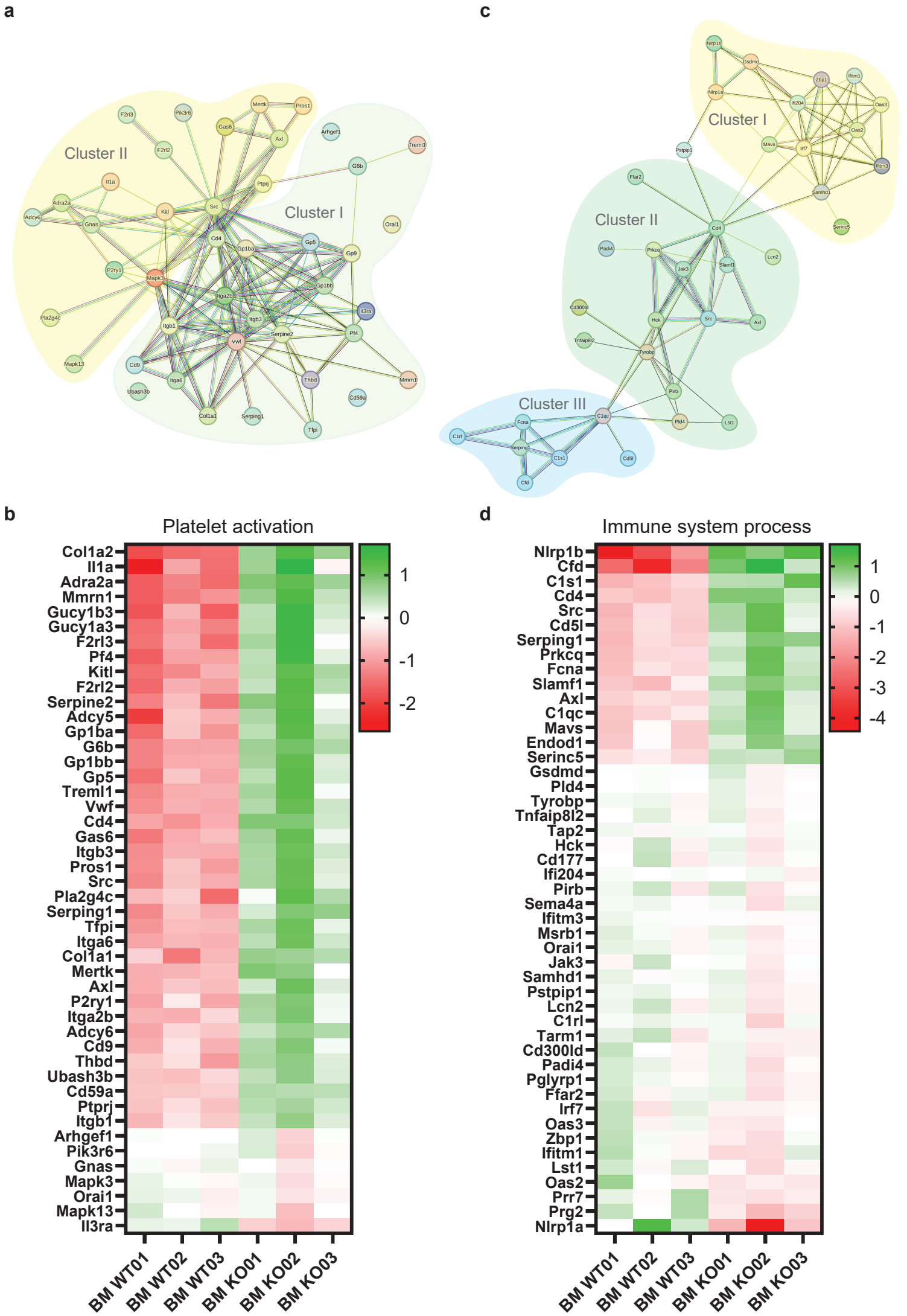
a
Cluster II
Cluster I
F2rl3
Pik3r6
Mertk
Pros1
Gas6
Axl
Arhgef1
Treml1
F2rl2
G6b
Il1a
Ptprj
Adra2a
Adcy6
Gnas
Kitl
Src
Orai1
Cd4
Gp5
Gp1ba
Gp9
P2ry1
Mapk3
Gp1bb
Itga2b
Il3ra
Pla2g4c
Itgb1
Itgb3
Serpine2
Pf4
Vwf
Mapk13
Cd9
Itga6
Thbd
Mmrn1
Ubash3b
Cd59a
Col1a1
Serping1
Tfpi
c
Cluster I
Cluster II
Cluster III
Nlrp1b
Gsdmd
Zbp1
Ifitm1
Nlrp1a
Ifi204
Oas3
Oas2
Mavs
Irf7
Ifitm3
Pstpip1
Samhd1
Serinc5
Ffar2
Cd4
Padi4
Prkcq
Lcn2
Jak3
Slamf1
Cd300ld
Hck
Src
Axl
Tnfaip8l2
Tyrobp
Pirb
Pld4
Lst1
C1qc
Fcna
C1rl
Serping1
C1s1
Cd5l
Cfd
b
Platelet activation
Col1a2
Il1a
Adra2a
Mmrn1
Gucy1b3
Gucy1a3
F2rl3
Pf4
Kitl
F2rl2
Serpine2
Adcy5
Gp1ba
G6b
Gp1bb
Gp5
Treml1
Vwf
Cd4
Gas6
Itgb3
Pros1
Src
Pla2g4c
Serping1
Tfpi
Itga6
Col1a1
Mertk
Axl
P2ry1
Itga2b
Adcy6
Cd9
Thbd
Ubash3b
Cd59a
Ptprj
Itgb1
Arhgef1
Pik3r6
Gnas
Mapk3
Orai1
Mapk13
Il3ra
1
0
-1
-2
BM WT01
BM WT02
BM WT03
BM KO01
BM KO02
BM KO03
d
Immune system process
Nlrp1b
Cfd
C1s1
Cd4
Src
Cd5l
Serping1
Prkcq
Fcna
Slamf1
Axl
C1qc
Mavs
Endod1
Serinc5
Gsdmd
Pld4
Tyrobp
Tnfaip8l2
Tap2
Hck
Cd177
Ifi204
Pirb
Sema4a
Ifitm3
Msrb1
Orai1
Jak3
Samhd1
Pstpip1
Lcn2
C1rl
Tarm1
Cd300ld
Padi4
Pglyrp1
Ffar2
Irf7
Oas3
Zbp1
Ifitm1
Lst1
Oas2
Prr7
Prg2
Nlrp1a
1
0
-1
-2
-3
-4
BM WT01
BM WT02
BM WT03
BM KO01
BM KO02
BM KO03

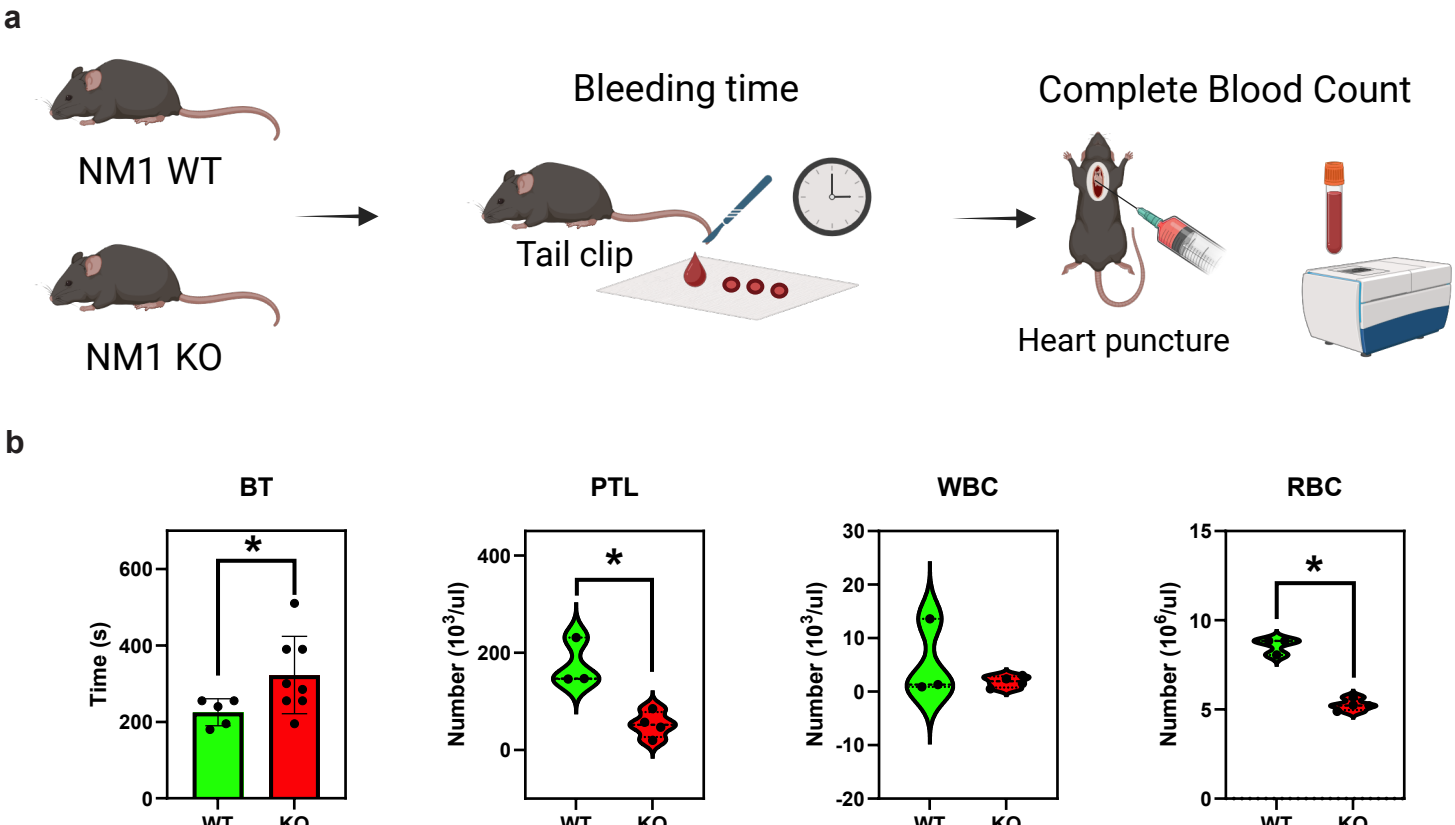
a
NM1 WT
NM1 KO
Bleeding time
Tail clip
Complete Blood Count
Heart puncture
b
BT
Time (s)
600
400
200
0
*
WT
KO
PTL
Number (10^3/ul)
400
200
0
*
WT
KO
WBC
Number (10^3/ul)
30
20
10
0
-10
-20
WT
KO
RBC
Number (10^6/ul)
15
10
5
0
*
WT
KO

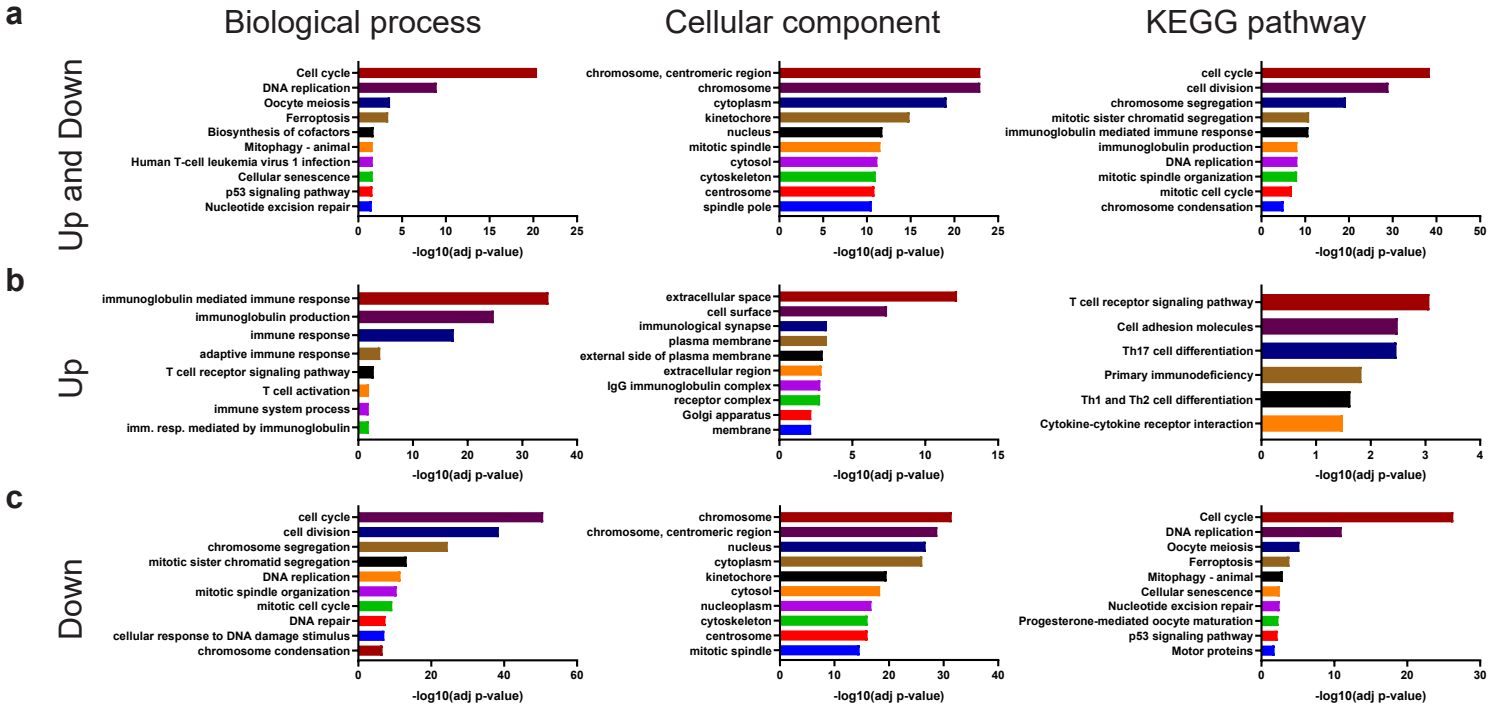
a
Biological process
Cellular component
KEGG pathway
Up and Down
Cell cycle
DNA replication
Oocyte meiosis
Ferroptosis
Biosynthesis of cofactors
Mitophagy - animal
Human T-cell leukemia virus 1 infection
Cellular senescence
p53 signaling pathway
Nucleotide excision repair
0 5 10 15 20 25
-log10(adj p-value)
chromosome, centromeric region
chromosome
cytoplasm
kinetochore
nucleus
mitotic spindle
cytosol
cytoskeleton
centrosome
spindle pole
0 5 10 15 20 25
-log10(adj p-value)
cell cycle
cell division
chromosome segregation
mitotic sister chromatid segregation
immunoglobulin mediated immune response
immunoglobulin production
DNA replication
mitotic spindle organization
mitotic cell cycle
chromosome condensation
0 10 20 30 40 50
-log10(adj p-value)
b
Up
immunoglobulin mediated immune response
immunoglobulin production
immune response
adaptive immune response
T cell receptor signaling pathway
T cell activation
immune system process
imm. resp. mediated by immunoglobulin
0 10 20 30 40
-log10(adj p-value)
extracellular space
cell surface
immunological synapse
plasma membrane
external side of plasma membrane
extracellular region
IgG immunoglobulin complex
receptor complex
Golgi apparatus
membrane
0 5 10 15
-log10(adj p-value)
T cell receptor signaling pathway
Cell adhesion molecules
Th17 cell differentiation
Primary immunodeficiency
Th1 and Th2 cell differentiation
Cytokine-cytokine receptor interaction
0 1 2 3 4
-log10(adj p-value)
c
Down
cell cycle
cell division
chromosome segregation
mitotic sister chromatid segregation
DNA replication
mitotic spindle organization
mitotic cell cycle
DNA repair
cellular response to DNA damage stimulus
chromosome condensation
0 20 40 60
-log10(adj p-value)
chromosome
chromosome, centromeric region
nucleus
cytoplasm
kinetochore
cytosol
nucleoplasm
cytoskeleton
centrosome
mitotic spindle
0 10 20 30 40
-log10(adj p-value)
Cell cycle
DNA replication
Oocyte meiosis
Ferroptosis
Mitophagy - animal
Cellular senescence
Nucleotide excision repair
Progesterone-mediated oocyte maturation
p53 signaling pathway
Motor proteins
0 10 20 30
-log10(adj p-value)

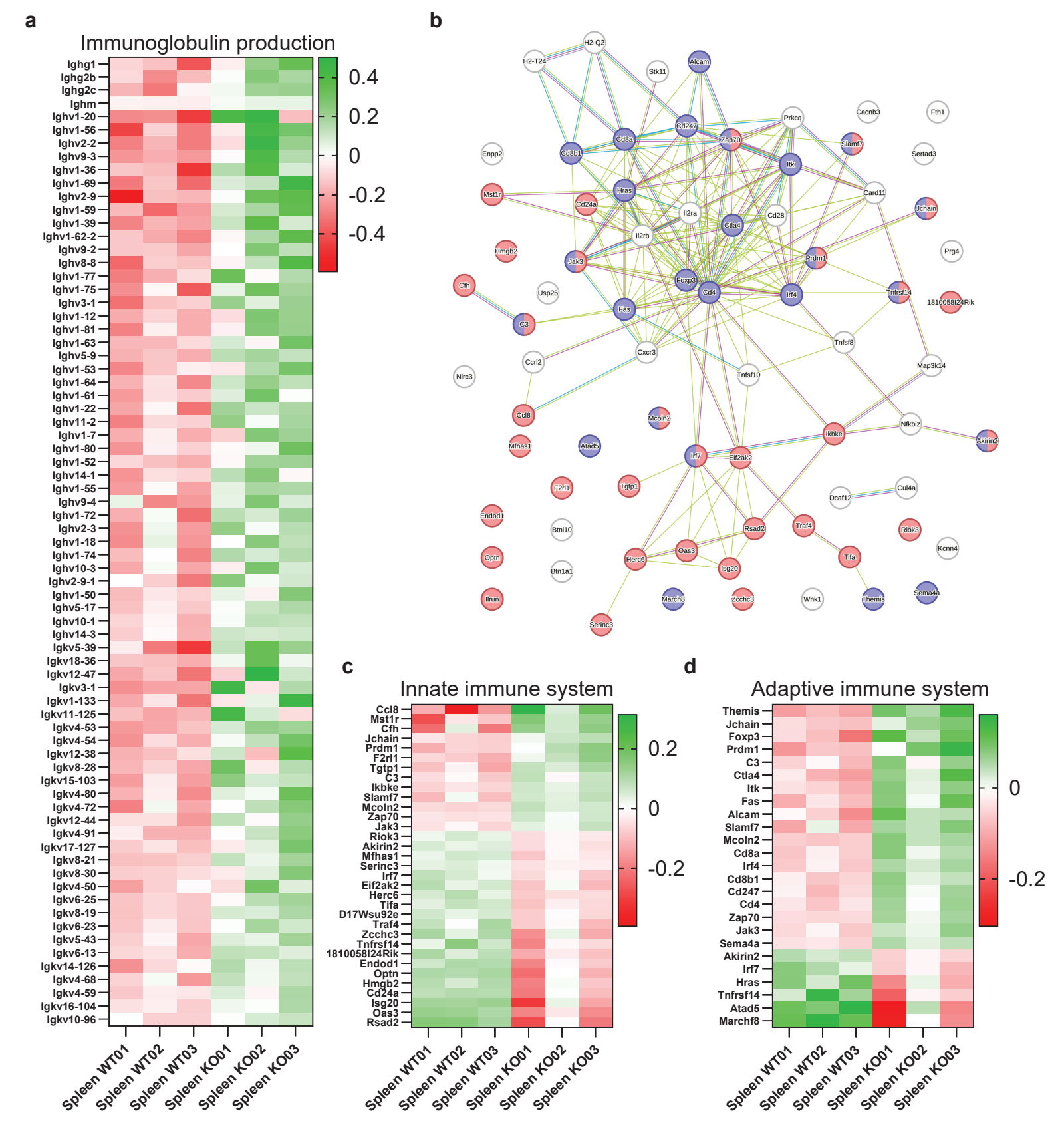
a
Immunoglobulin production
Ighg1
Ighg2b
Ighg2c
Ighm
Ighv1-20
Ighv1-56
Ighv2-2
Ighv9-3
Ighv1-36
Ighv1-69
Ighv2-9
Ighv1-59
Ighv1-39
Ighv1-62-2
Ighv9-2
Ighv8-8
Ighv1-77
Ighv1-75
Ighv3-1
Ighv1-12
Ighv1-81
Ighv1-63
Ighv5-9
Ighv1-53
Ighv1-64
Ighv1-61
Ighv1-22
Ighv11-2
Ighv1-7
Ighv1-80
Ighv1-52
Ighv14-1
Ighv1-55
Ighv9-4
Ighv1-72
Ighv2-3
Ighv1-18
Ighv1-74
Ighv10-3
Ighv2-9-1
Ighv1-50
Ighv5-17
Ighv10-1
Ighv14-3
Igkv5-39
Igkv18-36
Igkv12-47
Igkv3-1
Igkv1-133
Igkv11-125
Igkv4-53
Igkv4-54
Igkv12-38
Igkv8-28
Igkv15-103
Igkv4-80
Igkv4-72
Igkv12-44
Igkv4-91
Igkv17-127
Igkv8-21
Igkv8-30
Igkv4-50
Igkv6-25
Igkv8-19
Igkv6-23
Igkv5-43
Igkv6-13
Igkv14-126
Igkv4-68
Igkv4-59
Igkv16-104
Igkv10-96
0.4
0.2
0
-0.2
-0.4
Spleen WT01
Spleen WT02
Spleen WT03
Spleen KO01
Spleen KO02
Spleen KO03
b
H2-Q2
H2-T24
Stk11
Alcam
Prkcq
Cacnb3
Fth1
Cd247
Cd8a
Zap70
Slamf7
Enpp2
Cd8b1
Itk
Sertad3
Mst1r
Hras
Card11
Cd24a
Il2ra
Cd28
Jchain
Ctla4
Il2rb
Hmgb2
Prdm1
Prg4
Jak3
Foxp3
Cfh
Usp25
Cd4
Irf4
Tnfrsf14
1810058I24Rik
Fas
C3
Tnfsf8
Cxcr3
Ccrl2
Map3k14
Nlrc3
Tnfsf10
Ccl8
Mcoln2
Nfkbiz
Ikbke
Akirin2
Mfhas1
Atad5
Irf7
Eif2ak2
F2rl1
Tgtp1
Cul4a
Dcaf12
Endod1
Btnl10
Rsad2
Traf4
Riok3
Kcnn4
Optn
Oas3
Herc6
Tifa
Btn1a1
Isg20
Ilrun
March8
Zcchc3
Wnk1
Themis
Sema4a
Serinc3
c
Innate immune system
Ccl8
Mst1r
Cfh
Jchain
Prdm1
F2rl1
Tgtp1
C3
Ikbke
Slamf7
Mcoln2
Zap70
Jak3
Riok3
Akirin2
Mfhas1
Serinc3
Irf7
Eif2ak2
Herc6
Tifa
D17Wsu92e
Traf4
Zcchc3
Tnfrsf14
1810058I24Rik
Endod1
Optn
Hmgb2
Cd24a
Isg20
Oas3
Rsad2
0.2
0
-0.2
Spleen WT01
Spleen WT02
Spleen WT03
Spleen KO01
Spleen KO02
Spleen KO03
d
Adaptive immune system
Themis
Jchain
Foxp3
Prdm1
C3
Ctla4
Itk
Fas
Alcam
Slamf7
Mcoln2
Cd8a
Irf4
Cd8b1
Cd247
Cd4
Zap70
Jak3
Sema4a
Akirin2
Irf7
Hras
Tnfrsf14
Atad5
Marchf8
0
-0.2
Spleen WT01
Spleen WT02
Spleen WT03
Spleen KO01
Spleen KO02
Spleen KO03